NASA TECHNICAL TRANSLATION NASA TT F-13,277

INTAKE AND JET EFFECTS OF TWO LIFT FAN CONFIGURATIONS ON FLOW PAST A WING

H. Neppert

Translation of
"Zulauf- und Strahleinfluesse zweier
Hubgeblaesekonfigurationen auf die
Fluegelstroemung,"
Deutsche Gesellschaft fuer Luft- und Raumfahrt,
Symposium ueber Verkehrsflugtechnik der Zukunft,
Hamburg, West Germany, Jan. 29, 1970,
Paper No. 70-008, 50 pp.

N70-39849

(ACCESSION NUMBER)	(THRU)
55	1
(PAGES)	(CODE)
—	01
(NASA CR OR TMX OR AD NUMBER)	(CATEGORY)

FACILITY FORM 602

NATIONAL AERONAUTICS AND SPACE ADMINISTRATION
WASHINGTON, D. C. 20546 OCTOBER, 1970

NASA TT F-13,277

INTAKE AND JET EFFECTS OF TWO LIFT FAN CONFIGURATIONS ON FLOW PAST A WING

H. Neppert

ABSTRACT. Determination of the effect of forces and moments induced on the wing of a VTOL aircraft by intake and jet streams of two lift fan configurations on the flow past the wing. Pressure measurements conducted on two lift fan configurations on a semimodel in a 3-m wind tunnel at a constant incident flow velocity are described. Based on these pressure measurements, normal force and pitching moment distributions of the wing were determined for different ground distances. The results obtained for both lift fan configurations are compared and discussed. A70-24047.

1. Introduction

/2*

Forces and moments are induced on the wing of a VTOL aircraft by the intake and jet effects. These forces and moments must be analyzed and optimized. The following pressure measurements on lift fan configurations (Figures 1 and 2) compiled by the Defense Department of the Federal Republic of Germany contribute to the resolution of this task. The measurements were conducted by the AVA in Goettingen [Aerodynamic Testing Station, Goettingen] on a semimodel in a 3-m wind tunnel at constant incident flow velocity, which yielded a Reynolds number of approximately $7.6 \cdot 10^5$ on the basis of 1μ. The jet velocity was varied for $V/V_j = 0$; 0.2; 0.4; 0.6; and ∞. In addition, the effect of the ground distance was studied for H/D = 1.5; 3.0 and ∞.

---

* Numbers in the margin indicate pagination in foreign text.

The electric motors, which were connected with the fans by 60 cm long shafts, could be mounted either above or below; they were mounted above for the jet and pressure measurements, and were mounted above or eliminated completely when measuring the pressure without the jet effect, so that the effects of the flow for wing could be obtained (Section 5.4). The measurements were carried out over an open measurement range, and the results were not corrected.

The V_j-velocities were the basis for the V/V_j values, which were calculated without lateral wing flow and without dead water formation at the exhaust in the limited transverse section. The actual jet spreads are shown in Section 5.1.

The purpose of these experiments is to create the experimental bases for a theoretical explanation of the jet effect on the flow for wing and the wake so that they can subsequently be used for optimization calculations thereby eliminating expenditures of time and money for experiments.

2. Coordinate Systems

The forces and moments are given in the body axis system.

The instantaneous reference points are 0.25 l (local) and 0.25 l_μ (entire wing)

3. Symbols /3

Geometric values

F	Reference wing surface
b	Reference wing spread
s	Reference semispan
l	Local wing chord
l_μ	Reference wing chord
L	Length of fuselage

F_j Cross-sectional area of jet fan exhaust

H Distance from ground to reference plane of fuselage at center of rotation α

D Diameter of cross-sectional are of fan exhaust

De Effective diameter of all exhaust cross-sectional areas $\left[= \left(\frac{4 \Sigma F_j}{\pi} \right)^{\frac{1}{2}} \right]$

Aerodynamic values

α Angle of attack, based on reference plane of fuselage

ϑ Angle of longitudinal inclination, positive if the reference plane of the fuselage at the nose rotates about the horizontal axis ($\hat{=} \alpha$ when H/D = 1.5 and 3.0, for given measurements)

V Streamline flow velocity

q Dynamic pressure of incident flow ($= \rho/2 \cdot V^2$)

V_j Reference velocity of jet exhaust

V_j^* Local jet velocity

C_{po} Pressure coefficient for top of wing $\left[= \frac{P_o - P}{q} = 1 - \left(\frac{V_o}{V} \right)^2 \right]$

C_{pu} Pressure coefficient for underside of wing $\left[= \frac{P_u - P}{q} = 1 - \left(\frac{V_u}{V} \right)^2 \right]$

C_Z Normal force coefficient ($= Z/q \cdot F$), positive upward

C_{Zo} Normal force coefficient when $\alpha = 0°$

C_A Coefficient of lift ($\approx C_Z$ when α is small)

C_{Wi} Coefficient of induced resistance ($= Wi/q \cdot F$)

C_M Coefficient of rolling-moment ($= M/q \cdot F \cdot l\mu$)

C_{Mo} Coefficient of rolling-moment when $C_Z = 0$

α_0 Angle of attack when $C_Z = 0$

S Jet thrust when H/D = ∞

S_0 Jet thrust when V = 0 and H/D = ∞

ΔZ Jet-induced normal force (= $\Delta C_Z \cdot q \cdot F$)

ΔM Jet-induced rolling-moment (= $\Delta C_M \cdot q \cdot F \cdot l\mu$

4. Model Data (Cf. also Figure 2) /4

Wing Configuration A

F	= 0.908 m^2
Λ	= 6.00
λ	= 0.40
b	= 2.336 m
s	= 1.168 m
li	= 0.556 m
la	= 0.222 m
φ_{25}	= 30°
$l\mu$	= 0.413 m
X_{N25}	= 0.428 m
ε	= 1° to ref. plane of fuselage

Wing without warping
Profile NACA 65 A 212 const.

Wing Configuration B

F	= 1.126 m^2
Λ	= 4.85
λ	= 0.40
b	= 2.336 m
s	= 1.168 m
s_K	= 0.340 m
li	= 0.556 (0.845) m
la	= 0.222 m
φ_{25}	= 30°
$l\mu$	= 0.590 m
X_{N25}	= 0.380 m
ε	= 1° to ref. plane of fuselage

Wing without warping
Profile NACA 65 A 212 const. except s_K

Fan jet arrangements

Config. A (jet in ref. plane of fuselage)

6 X_6 = -0.600 m
Y_6 = 0.260 m

7 X_7 = +0.600 m
Y_7 = 0.260 m

Config. B (jet in ref. plane of wing)

4 X_4 = -0.310 m
Y_4 = 0.230 m

5 X_5 = +0.145 m
Y_5 = 0.230 m

Line of reference for X values: axis of rotation α

Line of reference for Y values: axis of the fuselage

Data on fans

D_a = 0.170 m; D_i = 0.085 m; F_j = 0.017 m^2 (transverse area)

$\Sigma F_j/F$ = 0.075 for Config. A

U_{max} = 27,000 1/min

$V/V_j = \infty$: Config. A without fan nacelles on the fuselage, in Config. B fan louvers closed.

5. Discussion of Results

/5

5.1 Jet Measurements

The thrusts integrated with respect to V_j^* when Z/D = 0 (in the reference plane of the fuselage) vary greatly between V = 0 and V $\neq$ 0. On the other hand, the α effect is very small. These thrusts are mean values from integrations of different circular sections of φ (Figure 3).

The effect of the hub in the formation of deadwater is comparatively obvious when V = 0 and V $\neq$ 0 (Figure 4). This reduction in thrust when V $\neq$ 0 is primarily the result of the fact that the downwash flow is more perturbed behind the hub. For this reason, a comparison of S/S_0 with those of a full-scale fan according to [1] and [2] yields poorer efficiencies for the model fan which could be improved by increasing the Reynolds number, changing the intake lips, and above all, the shape of the hub.

The characteristic distributions of V_j^* = const. in the sections where Z/D = 1 are calculated from the velocity distributions for different sections φ (Figure 5). In this instance, we can observe the familiar rolling-up of the jet by the lateral wing flow. The distortion produced when V/V_j = 0.6 is explained by

the fuselage effect; the nacelles of the landing gear were removed when the jet measurements were taken, and only the forward fan 4 was operating.

5.2 Pressure Measurements on Config. A

Several pressure distributions of the wing sections S_3, S_7 and S_{11} (compare Figure 2) are given for H/D = ∞, 3.0, and 1.5 (Figures 6 to 8). Both fans were always adjusted to the same rate of rotation. The primary factor for the jet effect on the flow for the wing is the change in the direction of the flow behind the first fan, which decreases toward the outside. As a result, the suction peak shifts near the fuselage to the underside, whereas it is usually located at the profile nose when incidence is positive. This effect is weakened when the distance to the ground is small through the directional effect of ground level.

The jet-induced C_p when V = 0 are based on the dynamic pressure which is produced by the constant incident velocity for all $V/V_j \neq 0$ values (Figure 8). It can be seen that, when V = 0, the jet has a slight effect on the upper surface of the wing only at the nose. On the undersurface of the wing, overpressures (fountain effect) and further inward, underpressures are produced by the collision of both fan jets and the deflection from the ground. This can be clearly seen from the isobar diagrams (Figure 9). Even the above-mentioned change in the direction of the incident flow caused by the jet effect can again be noticed, as a result of which the load is shifted further to the outside. /6

The distributions of the normal force and rolling-moment are obtained by integrating the local pressure distributions in the direction of the wing spread (Figures 10 and 11). It can be seen that, when H/D = ∞, the jet effect acts chiefly as a

warp for the direction of zero lift as can be seen from α_0. the $\partial c_z/\partial\alpha$ reduction behind the fan on the inboard wing and the increase on the outboard wing has not been explained (dipolar distribution); the inboard reduction might be explained by the reduction in the dynamic pressure with α as the submersion effect of the forward fan. A comparison of c_{z0}, which is strongly influenced by the jet, with another measurement shows good correlation according to [1]. Since, in this case, only the forward fan was operating, it can be ascertained, the rear fan probably has only a minimal effect on the flow for the wing. The inboard rolling-moments are subjected to an almost exclusively nose-heavy c_{m0} shift. Figure 12 shows the changes caused by the jet effect. Thus, for example, when the jet velocity is increased five times over the incident flow velocity, the inboard direction of zero lift deflects by $\Delta\alpha_0 \approx +12°$.

When H/D = 3.0 and 1.5 (Figures 13 and 14), the above-mentioned directional effect of the ground level generates smaller deviations in the jet effect than when the distance from the ground is greater. The values for $\partial c_z/\partial\alpha$ are also less affected by the jet than c_{z0}, but exhibit the familiar increases due to the ground effect. In contrast, the values for $\partial c_m/\partial c_z$, as opposed to those values when H/D = ∞, are more heavily influenced by the jet in this case, as the values for $\Delta\partial c_m/\partial c_z$ in Figure 15 show. In this case, the wingtips are shifted relatively near the ground (compare Figure 2) as a result of the geometry of the swept wing. This might be an explanation for the outboard deviations from the normal plotting of the aerodynamic centers (compare Figure 39).

When V = 0, the normal force distributions exhibit an inboard downwash as a result of the suction effect and an outboard lift as a result of the fountain effect caused by the

jet-induced C_p on the undersurface of the wing. In addition, the effect of the longitudinal inclination on the distribution of the normal force and the rolling-moments can be seen (Figures 16 and 17; reference q!).

When integrating for the entire wing, all coefficients are based on q_j when V = 0. When the longitudinal inclination is slightly negative, the jet induce minimum downwash on the wing (Figure 18). When V ≠ 0, the distance to the ground is great and the angle of attack is small, considerable downwash is generated by the jet.

When V = 0 and the distance to the ground is small, we obtain the greatest changes in the rolling-moments with ϑ (Figure 19), and these changes are obtained in a destabilizing sense by the forward shift of the fountain effect as ϑ is increased. According to [3], other configurations exhibit this tendency. On the other hand, when V ≠ 0, nose-heaviness is increased by the jet effect because the direction of the incident flow is deflected in such a way at the inboard sections of the swept wing which are in front of N_{25}, that in this case the direction of the incident flow is from above.

5.3 Pressure Measurements on Configuration B /7

Pressure distributions are given for the same cases as in Config. A (Figures 20 to 22). Similar distributions both calculated and theoretical can be found in [4] and [5]. It can be seen that in the case of Config. B, the jet influences the flow for the wing by the change in the direction of the incident flow which decreases toward the outside, as well as by direct changes in the velocity. High speeds are induced on the upper surface near the intake lips when V = 0. When V ≠ 0, these speeds are increased in the front, but reduced in the rear.

The different direction of the incident flow induces similar changes in the C_p distributions toward the outside as is the case for Config. A. These jet effects are again given in the isobar diagram (Figure 23).

For the normal force and rolling- moment distributions along the wing spread (Figures 24 and 25), the pressure distributions have been integrated to the edge of the fan louvers. Thus, all C_p which occur on the upper surface of the wing are taken into account. The moments for the inboard section are based on the 25% line for the original wing A (see Section 4).

It can be seen that inboard, there is a relatively large change in c_{m0} and $\partial c_m/\partial c_z$ by the jet effect (Figure 26). When the ground distance is small, and the jet speed high, the deviant curves for all the coefficients can be clearly seen (Figures 27 and 28), an effect which does not occur in the case of Config. A because of the greater distance between the jets (compare Figures 13 and 14). This can again be seen from the differences when $V/V_j = 0.2 = \text{const.}$ (Figure 29).

When V = 0 (reference q!), the lifts near the fans, induced by the overspeeds of the incident flow are obvious. The effect of the tail fans makes the inboard rolling-moments nose-heavy (Figures 30 and 31)

The integrations for the entire wing (Figures 32 and 33; reference pressure q and q_j) exhibit only positive, jet-induced normal forces when V = 0, and relatively small, negative normal forces when $V \neq 0$ and the distance to the ground is great, based on which, its dependence on the jet velocity is not as obvious as in the case of Config. A (compare Figure 18). When the ground distances are small, we obtain positive, jet-induced normal forces when H/D = 3.0 and negative ones when H/D = 1.5.

The rolling-moment curve is more stabile closer to the ground when V = 0 than for Config. A (compare Figure 19). The trim in this case becomes tail-heavy when V ≠ 0 as a result of the positive percentage of the inboard wing.

5.4 Comparison of Configurations A and B

The flows for the wing in the two configurations are affected differently by the jet (Figures 34 and 35). In Config. A, the effect is primarily indirect as a result of the change in the direction of the incident flow through the forward fan, which yields the negative Δc_{z0}. On the other hand, there is a smaller change in $\partial c_z/\partial\alpha$. In the case of Config. B, the outboard wing is influenced primarily by the change in the direction of the incident flow; the inboard wing, however, is also directly influenced by the changes in velocity near the fan. In this case, the local $\partial c_z/\partial\alpha$ is reduced more by the jet effect than in Config. A. /8

The curves plotted for Config. B when the ground distance is small are conspicuous. They can be explained by the immediate proximity of wing, ground and jet, which generates underpressures along the undersurface of the wing (injector effect; compare Figures 22 and 23). This effect is especially evident in hover (Figure 36). On the other hand, relatively large, positive Δc_z are produced inboard in this case by the incident flow to the fan.

$\Delta Z/S_0 \approx +0.04$ for Config. B (Figure 37) when in hover near the ground, but ≈ -0.04 for Config. A. Configuration B is also more advantageous in transition. With respect to the longitudinal stability, irregularly rising rolling-moments are produced in hover by the jet effect, especially when the ground distance is small and there is a positive change in ϑ.

This instability is less for Config. B than for Config. A (Figure 38).

A comparison of the $\Delta Z/S_0$ with force measurements according to [2] correlates well for transition in Config. A (Figure 37). According to this source, when $H/D = \infty$, it is more advantageous to mount the fan lower. The force measurements are only valid for forward fan positions, but they seem comparable according to the statement in Section 5.2, according to which it is almost exclusively the forward fan which has an effect on the flow for the wing. In the case of Config. B the comparison is only approximately valid. It must be taken into account that the force measurements are valid for the entire model and that these results are integrations of pressure measurements only of the wing to the side wall of the fuselage. The force measurements show the unfavorable effect of the forward fan ($\Delta\alpha_0 \rightarrow \Delta c_{z0}$) as well as the favorable effect of the tail fan (jet-flap effect). Whereas in Config. B, the unfavorable effects of the forward fan and the favorable effects of the tail fan cancel each other out, the unfavorable effect of the forward fan is much stronger in Config. A. Another advantage of Config. B over Config. A is the small trim from the jet effect, especially when the ground distance changes in transition (Figure 38). It should theoretically also be much simpler to counteract engine failure in this case. In addition, advantages with regard to installation and with regard to weight are also to be expected. Earlier burbling and a reduction of the $Ma_{crit.}$ as well as an increase in induced resistance as a result of the wing contour flaw when the c_a load is great would probably be disadvantageous (Figure 40).

When the C_A are equal: $(Wi_B/Wi_A)_{Ma = 0.9} \approx 1.5$; this means approximately 50% more induced resistance for Config. B while cruising. In a realistic comparison with equal lift (= total

weight) the differences become considerably smaller, because Config. B flies with less C_A because of its greater wing surface.

The aerodynamic centers indicate without jet effect the typical curves for swept wings (Figure 39). The jet effect produces slight backward shifts inboard in Config. A, but greater one in Config. B. In addition, the outboard aerodynamic centers in Config. A deviate from the normal curve in close proximity to the ground, when the jet speed is high. It is not certain whether this is conditioned by measurement errors or jet-induced ground effects. /9

The measured lift distributions without jet effect were compared with the calculated values in [6] (Figure 40). The Reynolds number is not enough to explain the relatively small $\partial c_z/\partial\alpha$. Since approximately the same deviations occur in both configurations, it is suspected that the flow in the measurement range is so perturbed by the symmetry plate, the undercarriage and the electric motors that the reference pressure no longer coincides with that in the measurement range. When $\partial_{Cz}/\partial\alpha$ are small for the entire wing, it must also be taken into account that the measurement results are only integrated to the side wall of the fuselage, but are then reference to the total F.

The electric motor effect causes a change in the increase in the lift as well as a greater inboard zero displacement as a result of the fact that the additional dynamic air pressure above the upper surface of the wing reduces the circulation. By assuming that this effect is the same for different jet velocity conditions, since the measurements were made at a constant incident flow velocity as well as with the motors mounted in the same position, the effect can be eliminated for the Δ values. Useable changes in the normal force and

rolling-moment distributions as a result of the jet effect were sought after in this investigation in accordance with the purpose of the study (see Section 1).

6. Summary

Normal force and rolling-moment distributions for the wing were calculated from pressure measurements at different ground distances for two lift fan configurations. Because these results depended on the jet velocity ratio, the jet was investigated first. The results of the pressure measurements are conditioned by the stagnation effect of the electric motors, as well as by the probable errors in the reference pressure which should be approximately the same for all coherent measurements and thus, in this case do not invalidate the differences sought by the jet effect. All the coefficients, in sufficient agreement with the force measurements for Config. B, indicate that there are advantages over Config. A with regard to the jet-induced normal force and rolling-moment.

REFERENCES /10

[1] Hall, P., Hickey, H., Kirk, J. V., Aerodynamic Characteristics of a Large Scale V/STOL Transport Model with Lift and Lift-Cruise Fans, NASA TN D - 4092.

[2] Hickey, D. H., Cook, W. L., Aerodynamics of V/STOL Aircraft Powered by Lift Fans, AGARD CP No. 22, September, 1967.

[3] Seibold, W., "Investigations on the Secondary Forces Produced by VTOL Fan Jets", Jahrbuch 1962 der WGLR.

[4] Wardlaw, R. L., McEachern, N. V., A Wing-Submerged Lifting Fan: Wind Tunnel Investigations and Analysis of Transition Performance, NRC of Canada AR LR - 243.

[5] McEachern, N. V., Currie, M. M., A Vortex Lattice Lifting Surface Theory for Wings with Submerged Fans, NRC of Canada AR LR - 311.

[6] Weissinger, J., "On an Expansion of the Prandtl Theory of the Support Line", Math. Nachrichten, Vol. 2, 1949.

Translated for the National Aeronautics and Space Administration under contract No. NASw-2038 by Translation Consultants, Ltd., 944 South Wakefield Street, Arlington, Virginia 22204.

REPRODUCIBILITY OF THE ORIGINAL PAGE IS POOR.

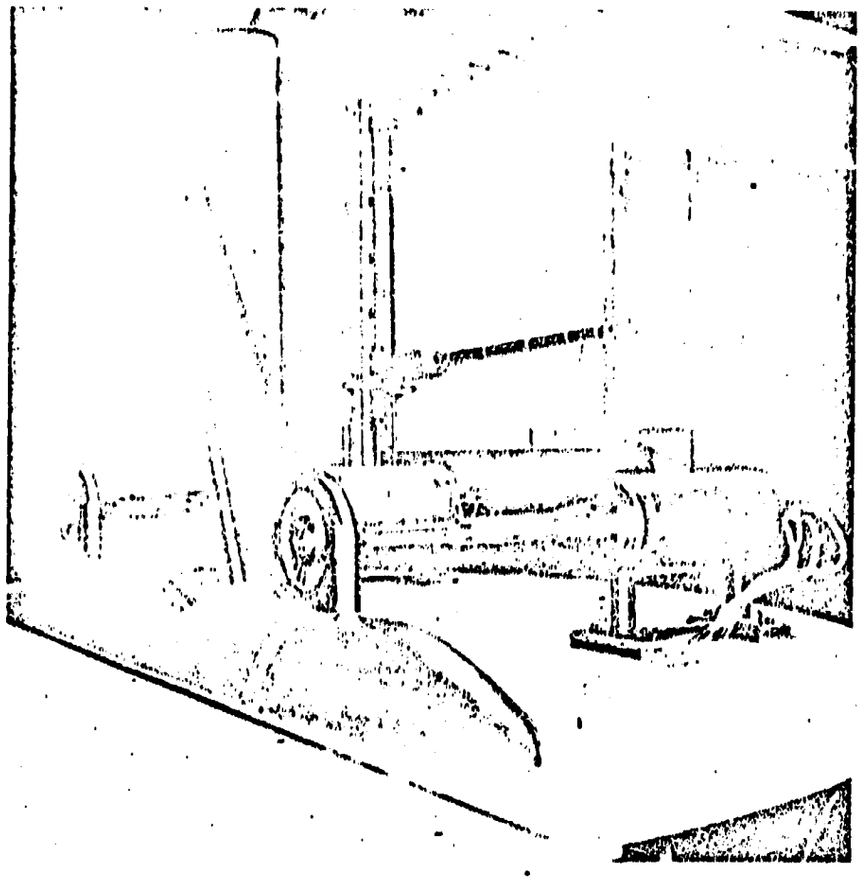

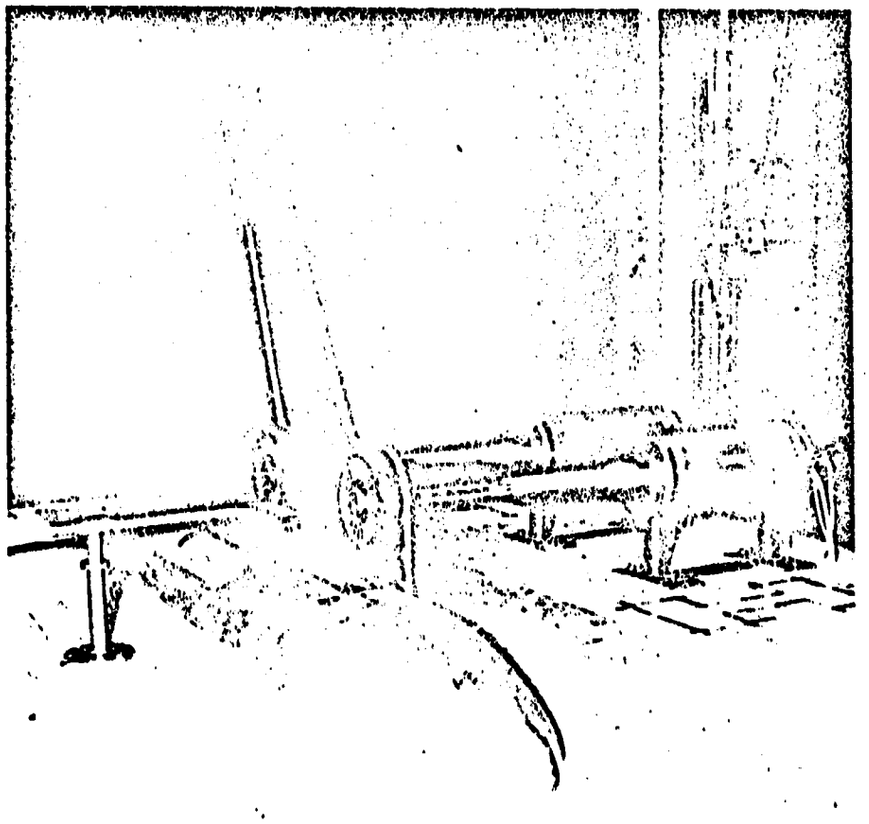

Above: Config. A

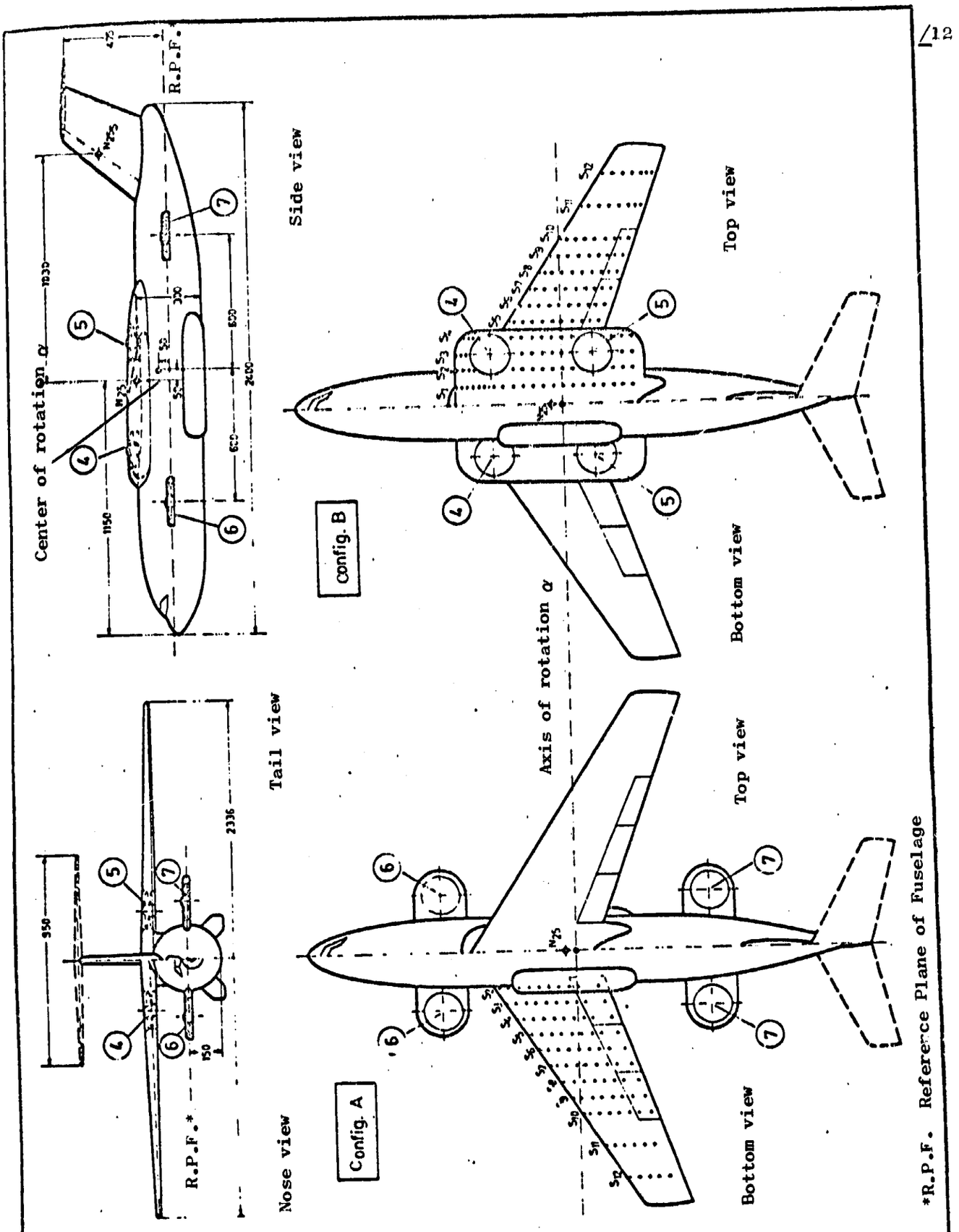

Fig. 2 Diagram of Configurations

Fig. 3

Jet measurements Config. B

$S, S_o = f\left(\frac{V_j}{V}, V_j\right)$ for $\frac{Z}{D} = 0$; $\frac{H}{D} = \infty$

H/B

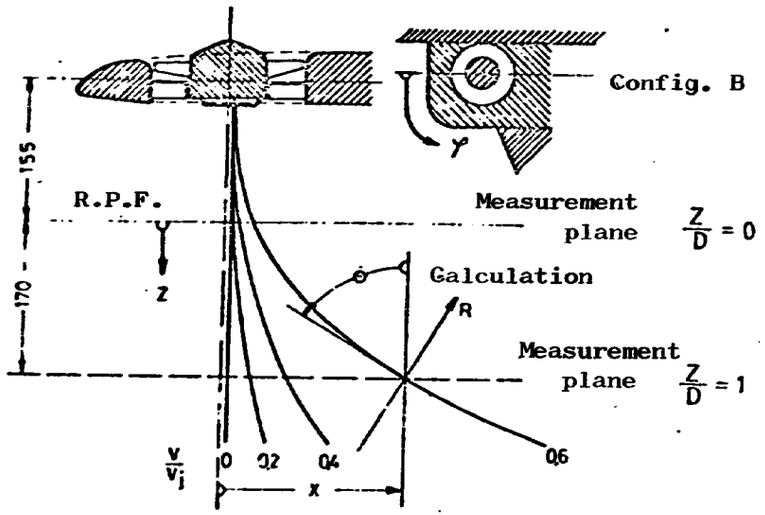

$\frac{V}{V_j} = 0$	$\frac{V_j}{V} = \infty$	V = 0 [m/s]	V_j = 133,5; 66,7; 44,3 [m/s]
0,2	5,0	25,7	133,5
0,4	2,5	25,7	66,7
0,6	1,67	25,7	44,3
∞	0	25,7	0

} calculated for V=0 (transverse section)

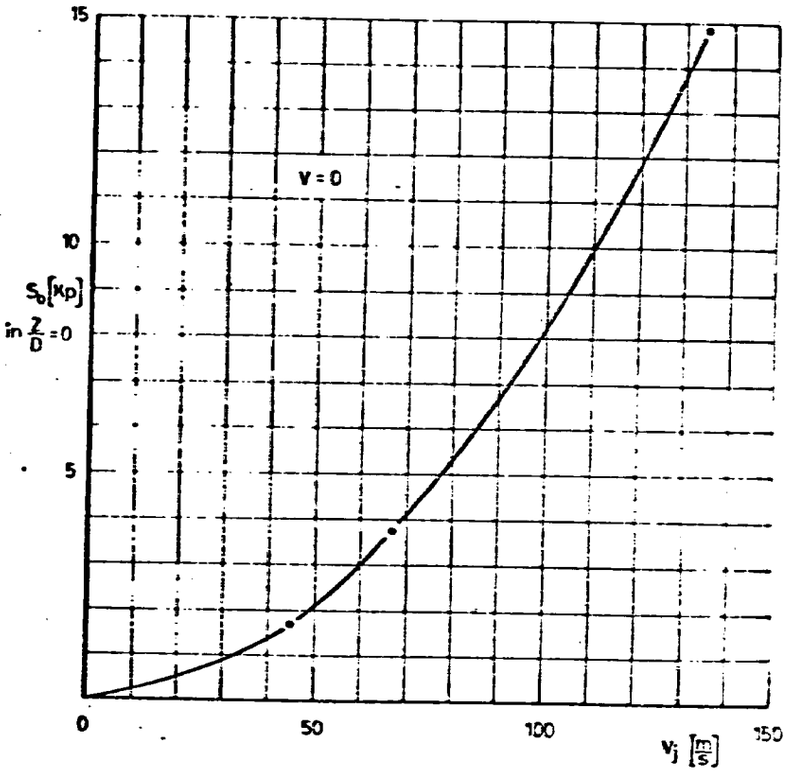

Hover H/D=∞

S [kp] in $\frac{Z}{D}$ = 0

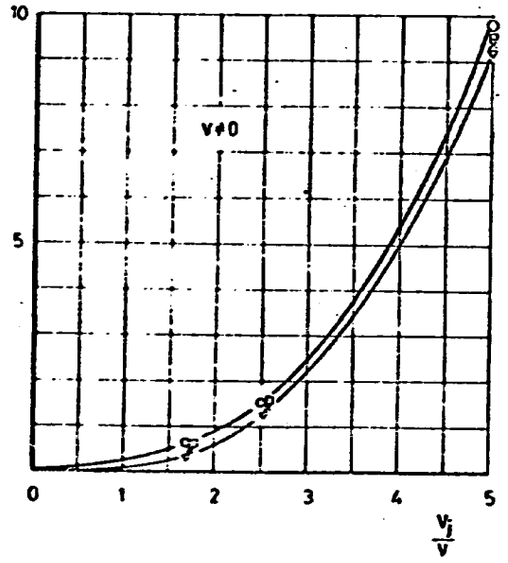

α = 0° ○
4° □
8° ×
12° ▽

Transition H/D=∞

[Commas represent decimal points]

Fig. 4

Jet measurements Config. B

$v_j^* = f(R)$ for $\frac{Z}{D} = 0$ and 1; $\frac{H}{D} = \infty$

HFB

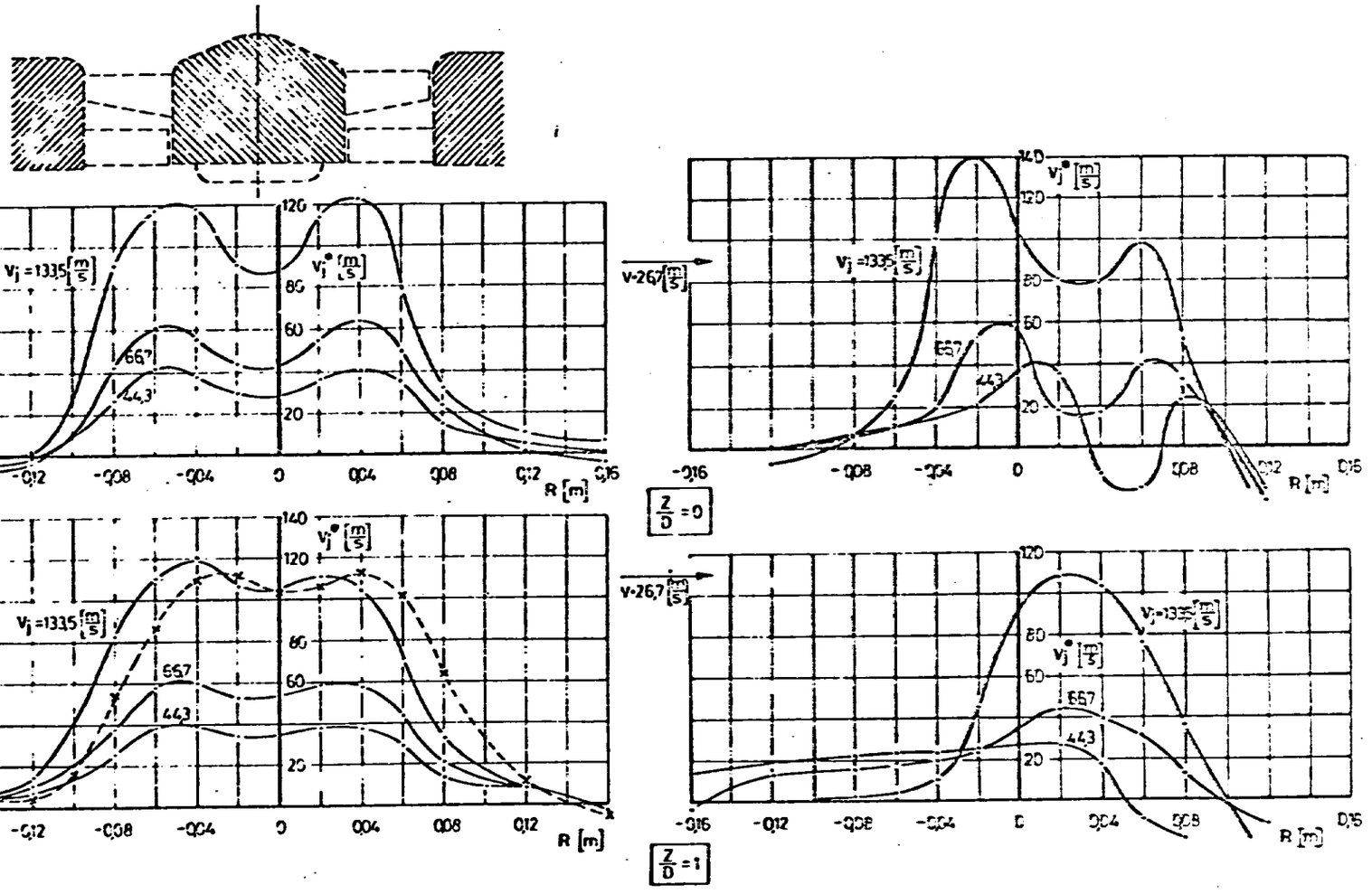

$\frac{v}{v_j} = 0$

$\alpha = 0°$

$\varphi = 0° —\ 90° ----$ (cf. Fig.3)

$\frac{v}{v_j} = 0{,}2\ ;\ 0{,}4\ ;\ 0{,}6$

$\alpha = 0°$

$\varphi = 0°$

[Commas represent decimal points]

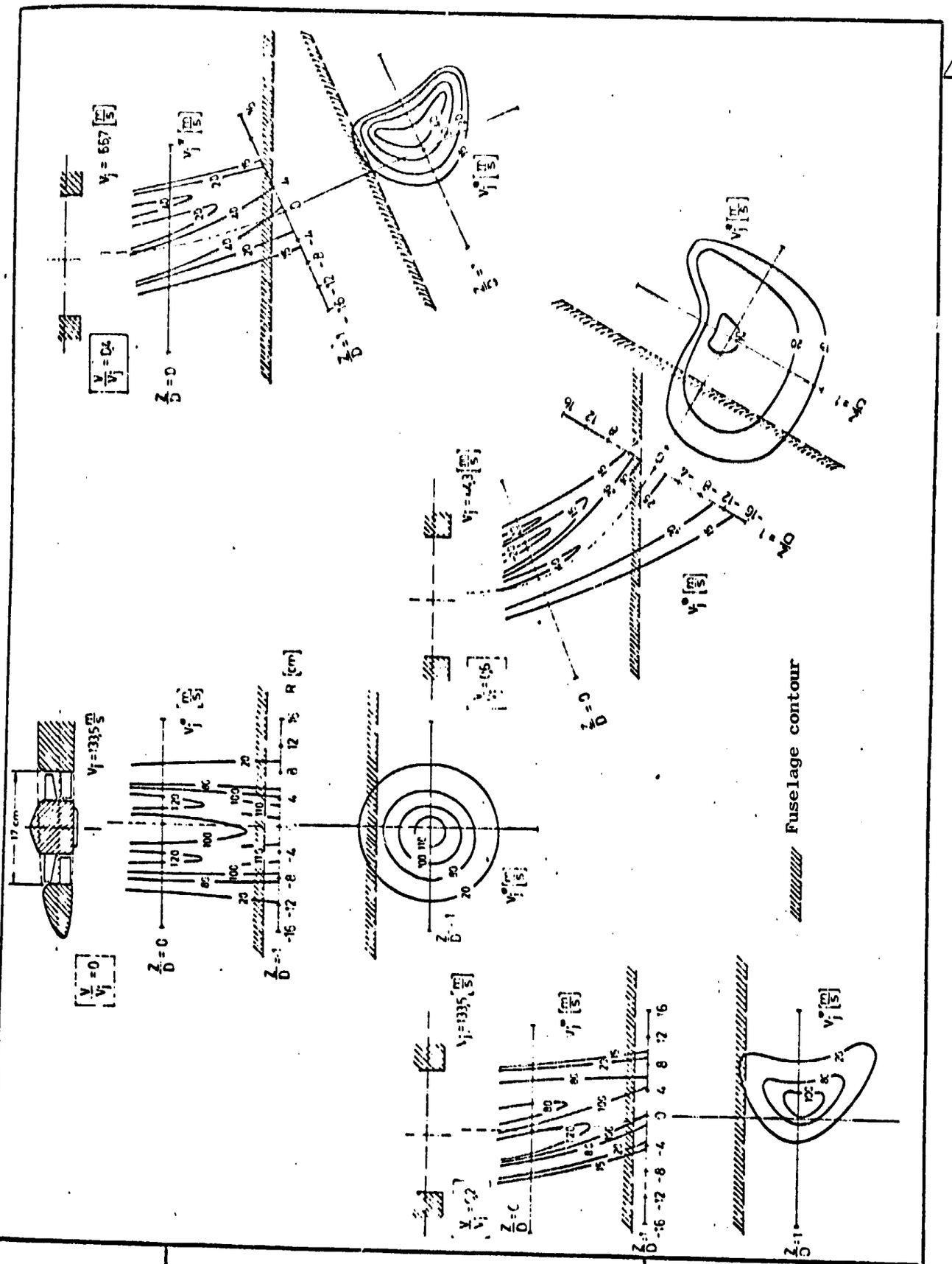

Fig. 5 — Jet measurements Config.B
$V^{\bullet}_{j\,konst.} = f(R)$ for $\varphi = 0$ and $R\varphi$; $\frac{H}{D} = \infty$

HFB

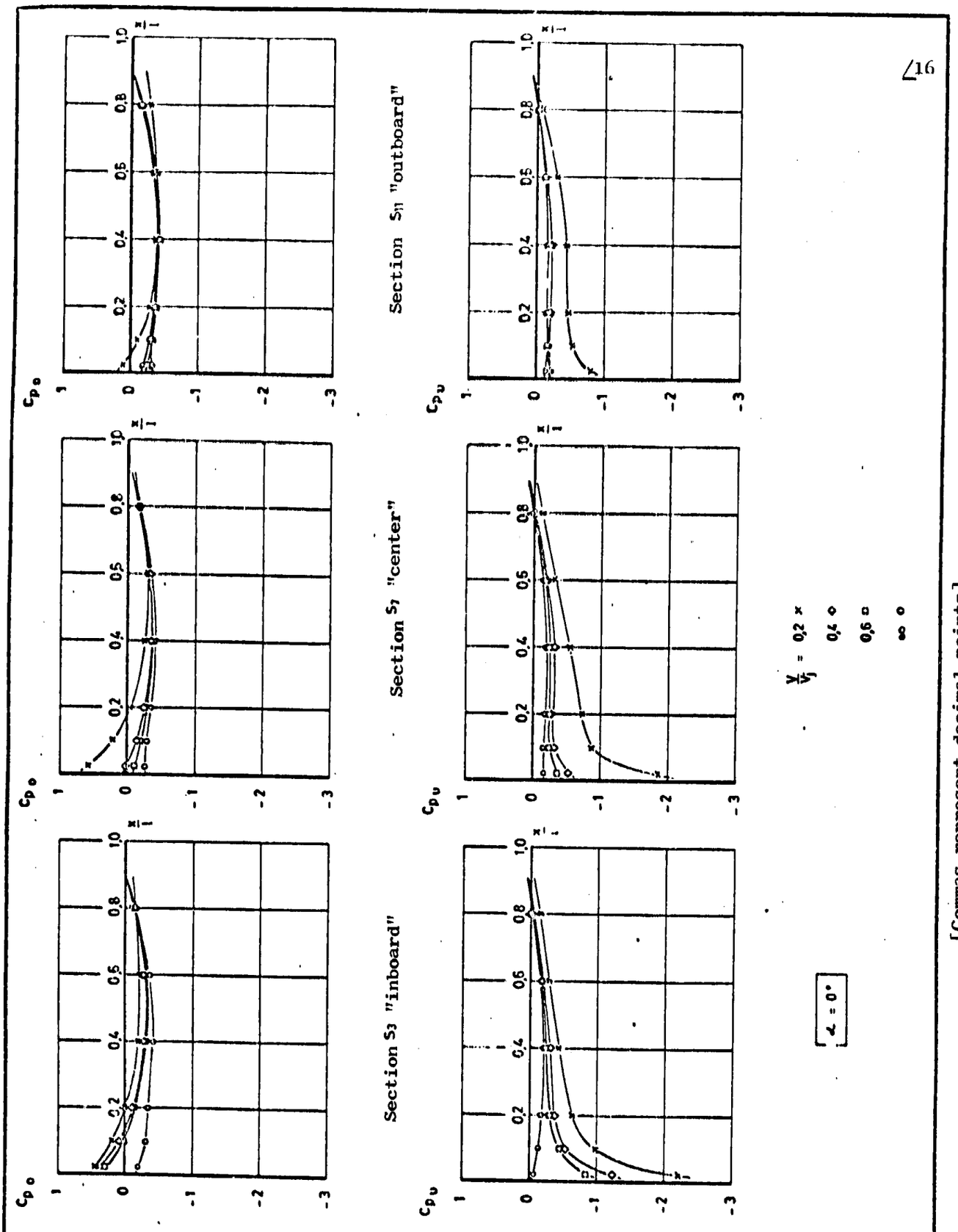

[Commas represent decimal points]

Fig. 6

Pressure measurements Config. A

$C_p = f\left(\frac{x}{l}\right)$ for $\frac{H}{D} = \infty$

HFB

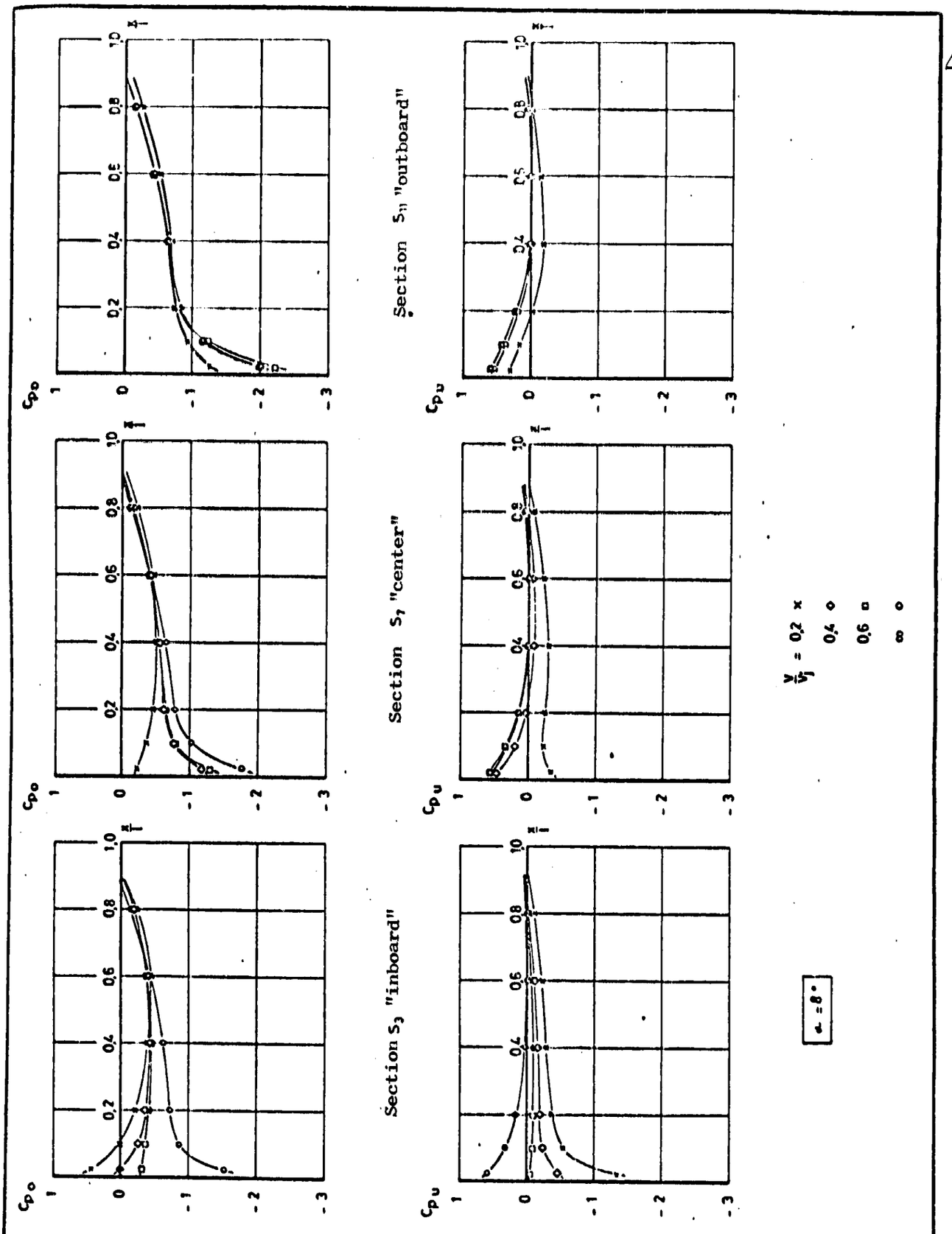

[Commas represent decimal points]

Fig. 7

Pressure measurements Config. A

$C_p = f\left(\frac{x}{l}\right)$ for $\frac{H}{D} = \infty$

HFB

Fig. 8

Pressure measurements Config. A

$C_p = f\left(\frac{x}{l}\right)$ for $\frac{H}{D} = 3,0$ & 1,5

HFB

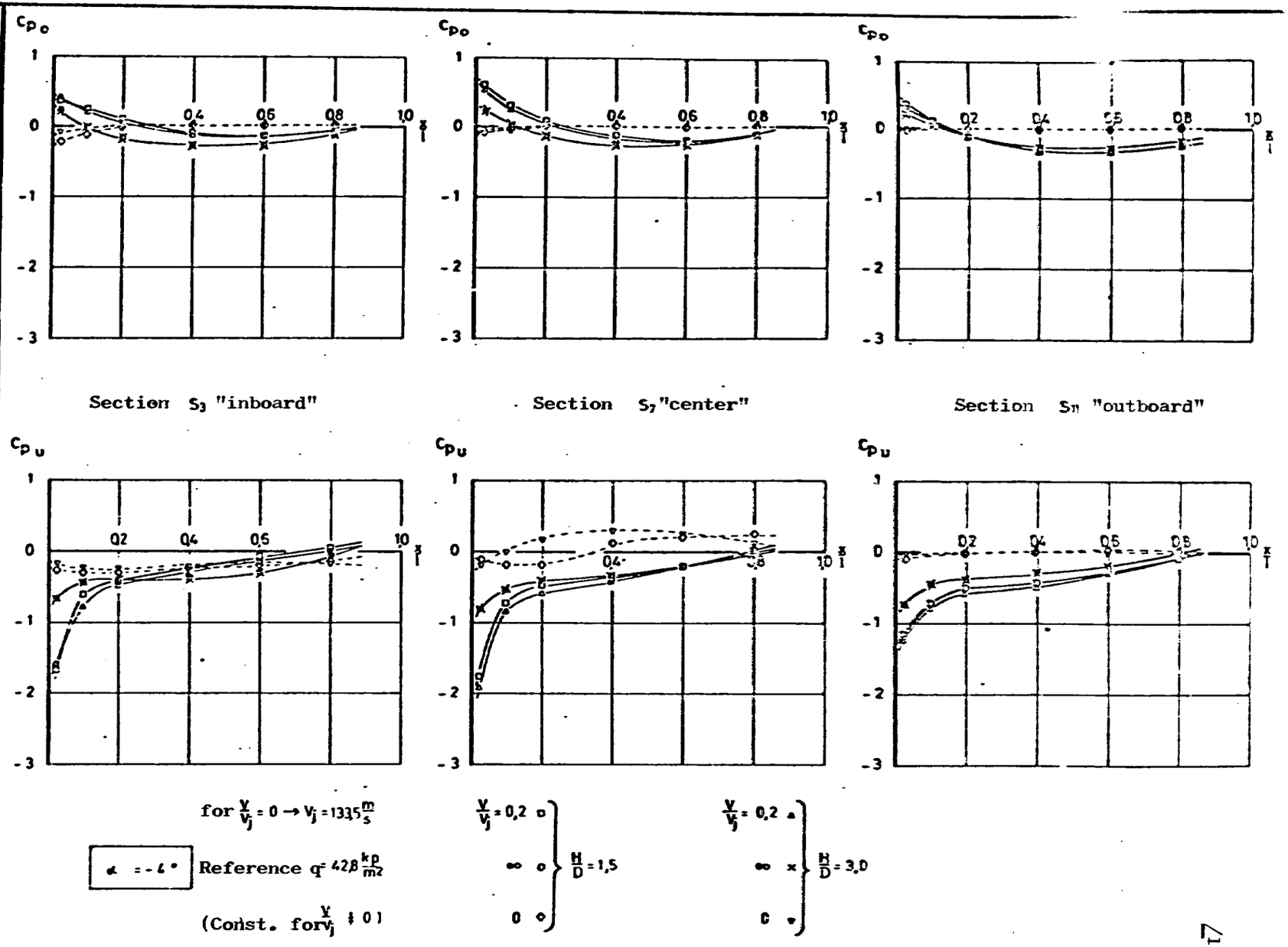

718

[Commas represent decimal points]

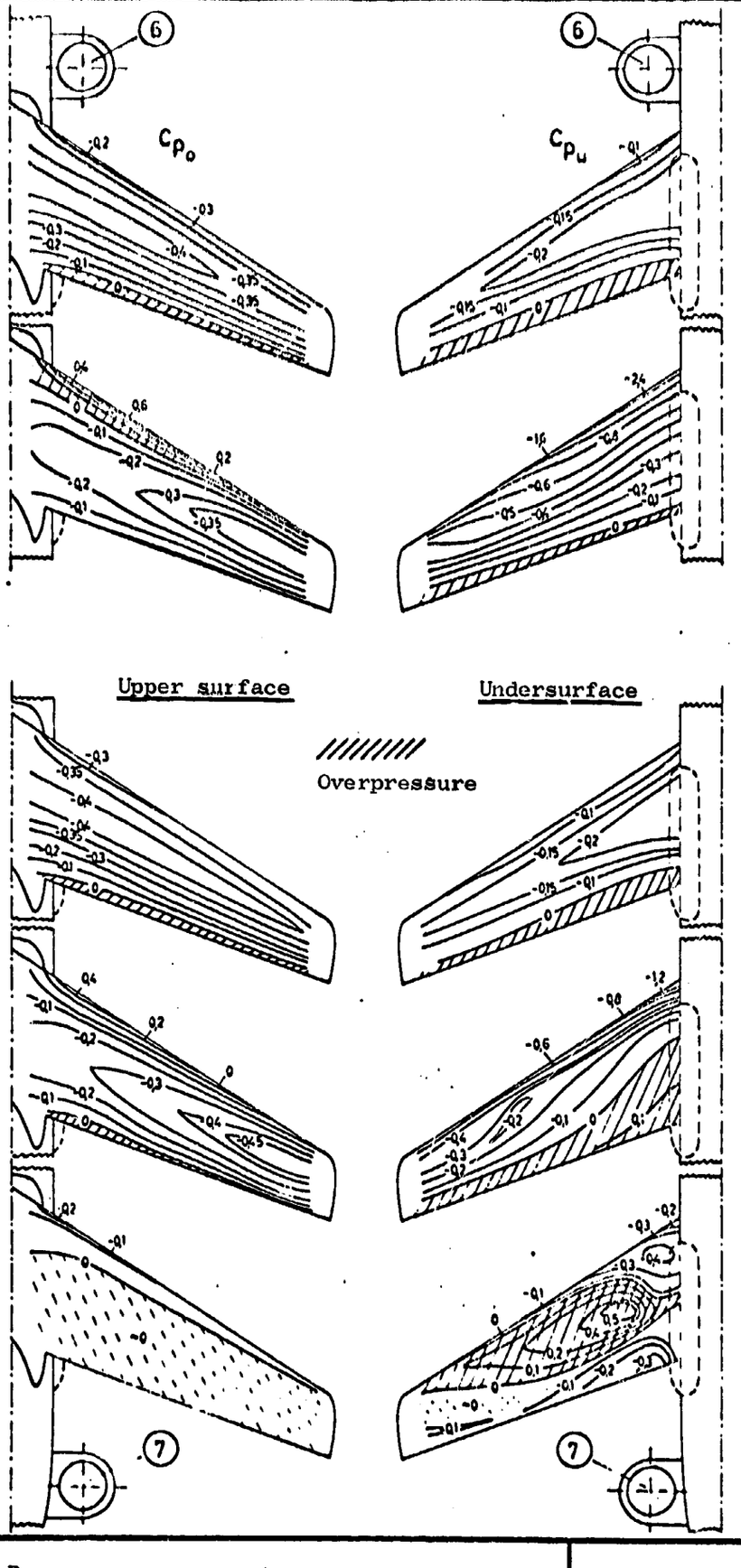

$$C_{p_{o,u}} = \frac{p_{o,u} - p}{q}$$

for $\frac{V}{V_j}=0$:

$V=0\ \frac{m}{s}$; $V_j=133.5\ \frac{m}{s}$

Reference $q=42.8\ \frac{kp}{m^2}$

(Const. for $\frac{V}{V_j} \neq 0$)

[Commas represent decimal points]

Fig. 9

Pressure measurements Config. A

Isobar distribution for α and $\vartheta = 0°$

HFB

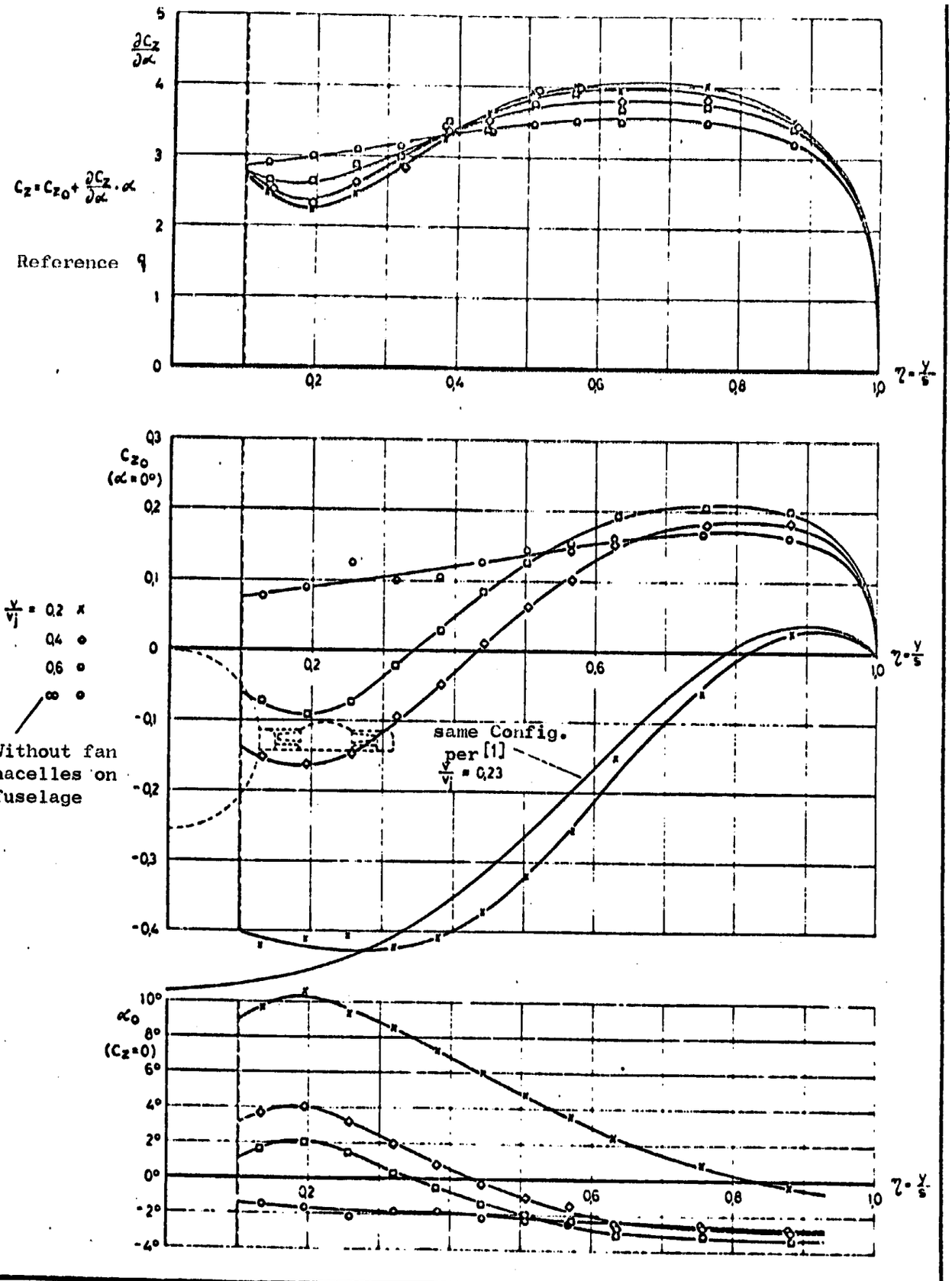

[Commas represent decimal points]

Fig. 10	Pressure measurements Config. A $\frac{\partial C_z}{\partial \alpha}, C_{z_0}, \alpha_0 = f(\eta)$ for $\frac{H}{D} = \infty$	HFB

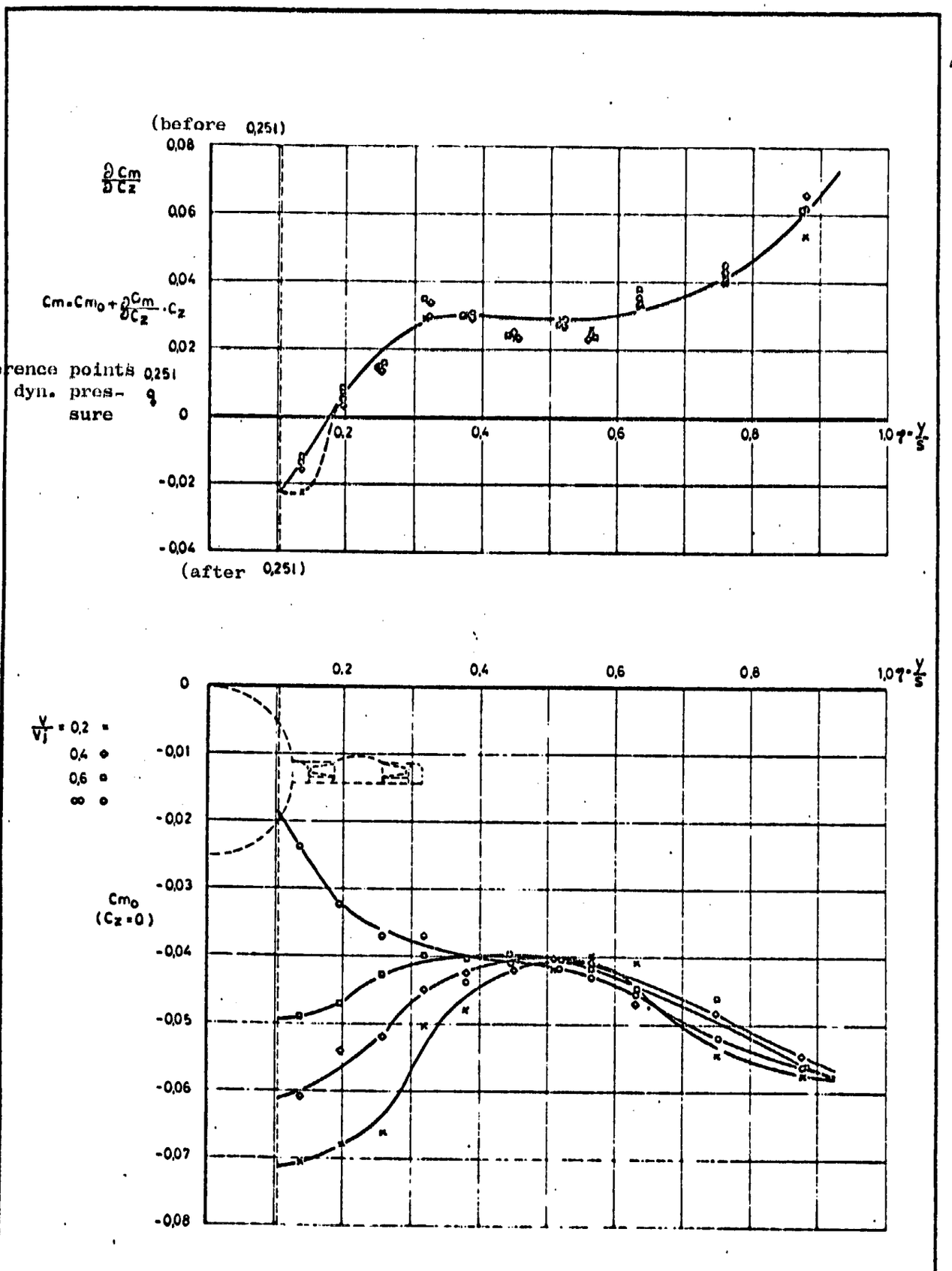

Fig. 11	Pressure measurements Config. A $\frac{\partial Cm}{\partial Cz}$, $Cm_0 = f(\eta)$ for $\frac{H}{D} = \infty$	HFB

[Commas represent decimal points]

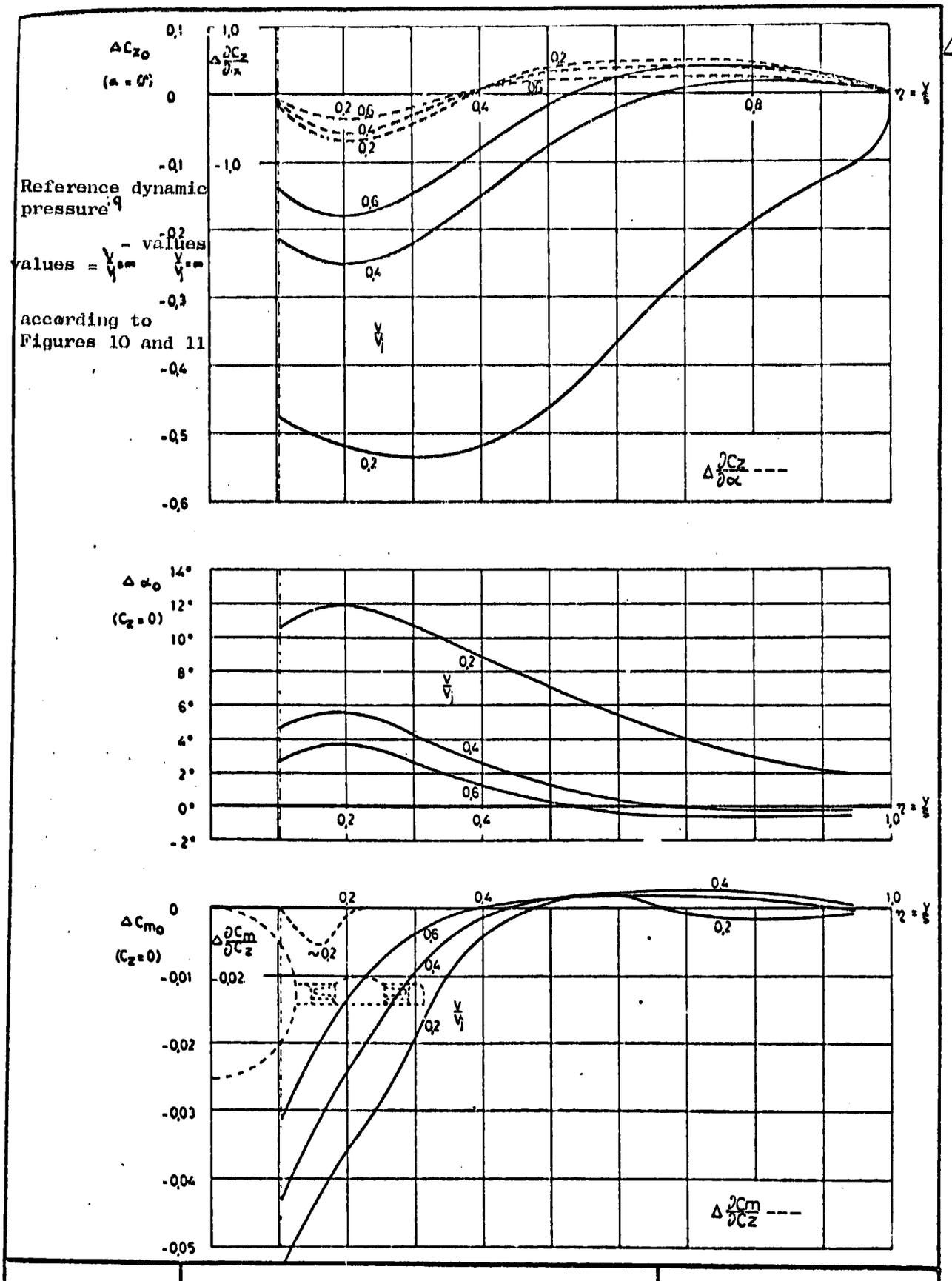

Reference dynamic pressure q

Δ values = $\frac{v}{v_j}$ - values $\frac{v}{v_j}$ =

according to Figures 10 and 11

[Commas represent decimal points]

Fig. 12	Pressure measurements Config. A ΔC_{z0}; $\Delta \frac{\partial C_z}{\partial \alpha}$; $\Delta \alpha_0$; C_{m0}; $\Delta \frac{\partial C_m}{\partial C_z} = f(\eta)$ for $\frac{H}{D} = \infty$	HFB

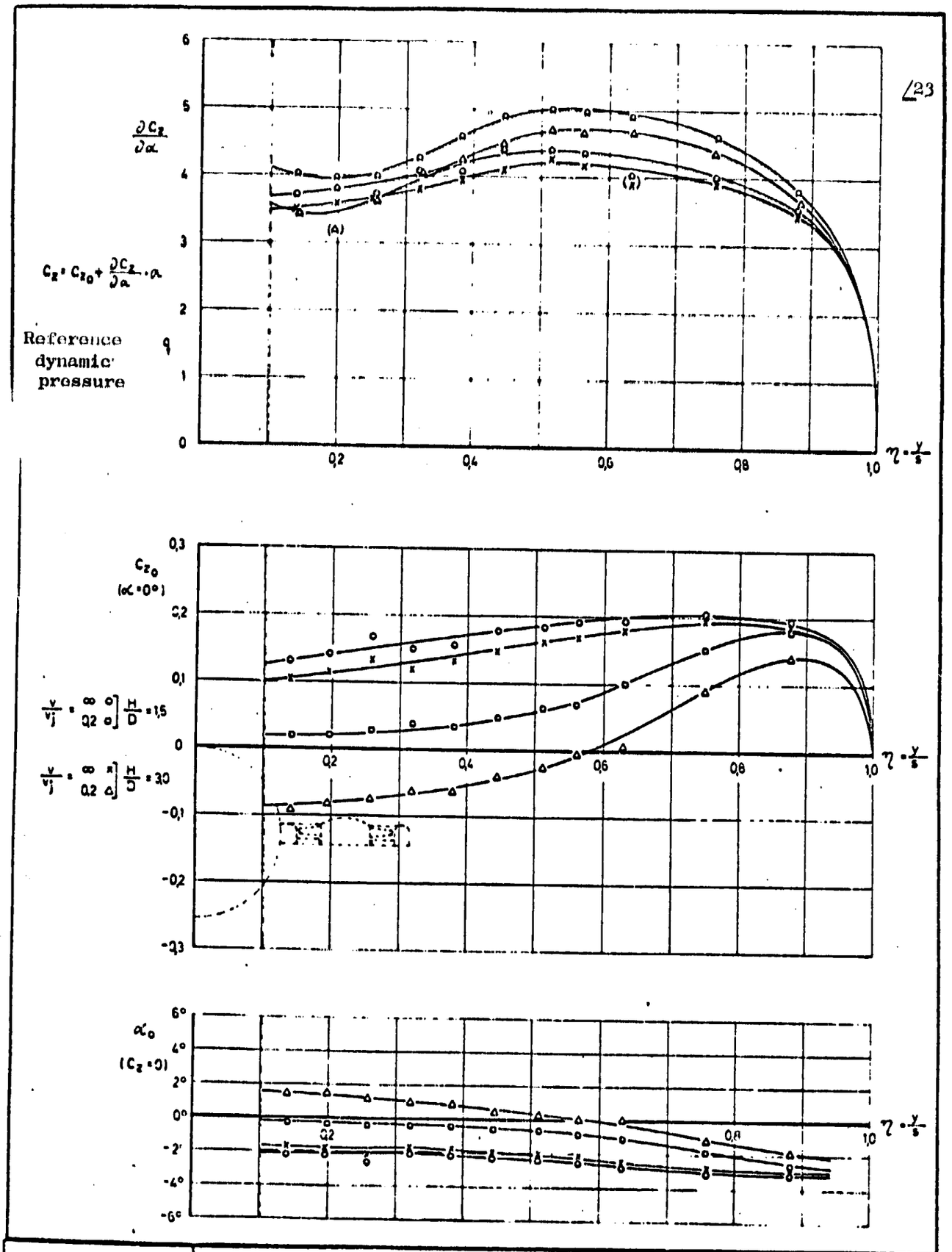
∠23
$\frac{\partial C_z}{\partial \alpha}$
$C_z = C_{z_0} + \frac{\partial C_z}{\partial \alpha} \cdot \alpha$
Reference dynamic pressure
q
$\eta = \frac{y}{s}$
C_{z_0} ($\alpha = 0°$)
$\frac{v}{v_j} = \infty$ ○ 0,2 ○ $\frac{H}{D} = 1,5$
$\frac{v}{v_j} = \infty$ × 0,2 △ $\frac{H}{D} = 3,0$
α_0 ($C_z = 0$)

[Commas represent decimal points]

Fig. 13	Pressure measurements Config. A $\frac{\partial C_z}{\partial \alpha}$; C_{z_0} ; $\alpha_0 = f(\eta)$ for $\frac{H}{D} = 3,0; 1.5$	HFB

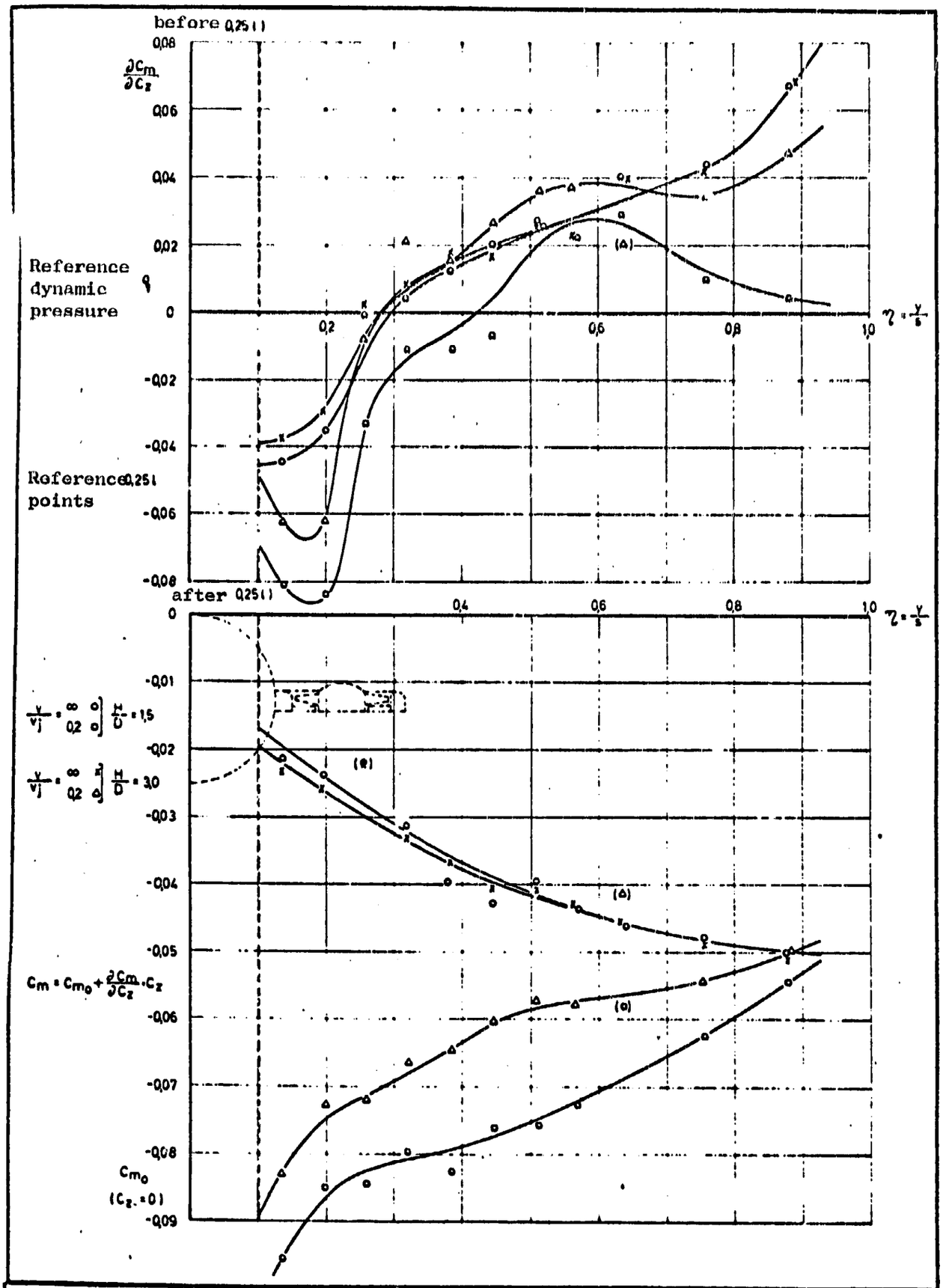
before 0,25 l
after 0,25 l
$\frac{\partial C_m}{\partial C_z}$
Reference dynamic pressure q
Reference points
$\eta = \frac{y}{s}$
$\frac{v}{v_j} = \infty$ 0,2 ○ ○ $\frac{H}{D} = 1,5$
$\frac{v}{v_j} = \infty$ 0,2 △ △ $\frac{H}{D} = 3,0$
$C_m = C_{m_0} + \frac{\partial C_m}{\partial C_z} \cdot C_z$
C_{m_0} ($C_z = 0$)

[Commas represent decimal points]

28	Fig. 14	Pressure measurements Config. A $\frac{\partial C_m}{\partial C_z}$, $C_{m_0} = f(\eta)$ for $\frac{H}{D} = 3,0$; 1,5	HFB

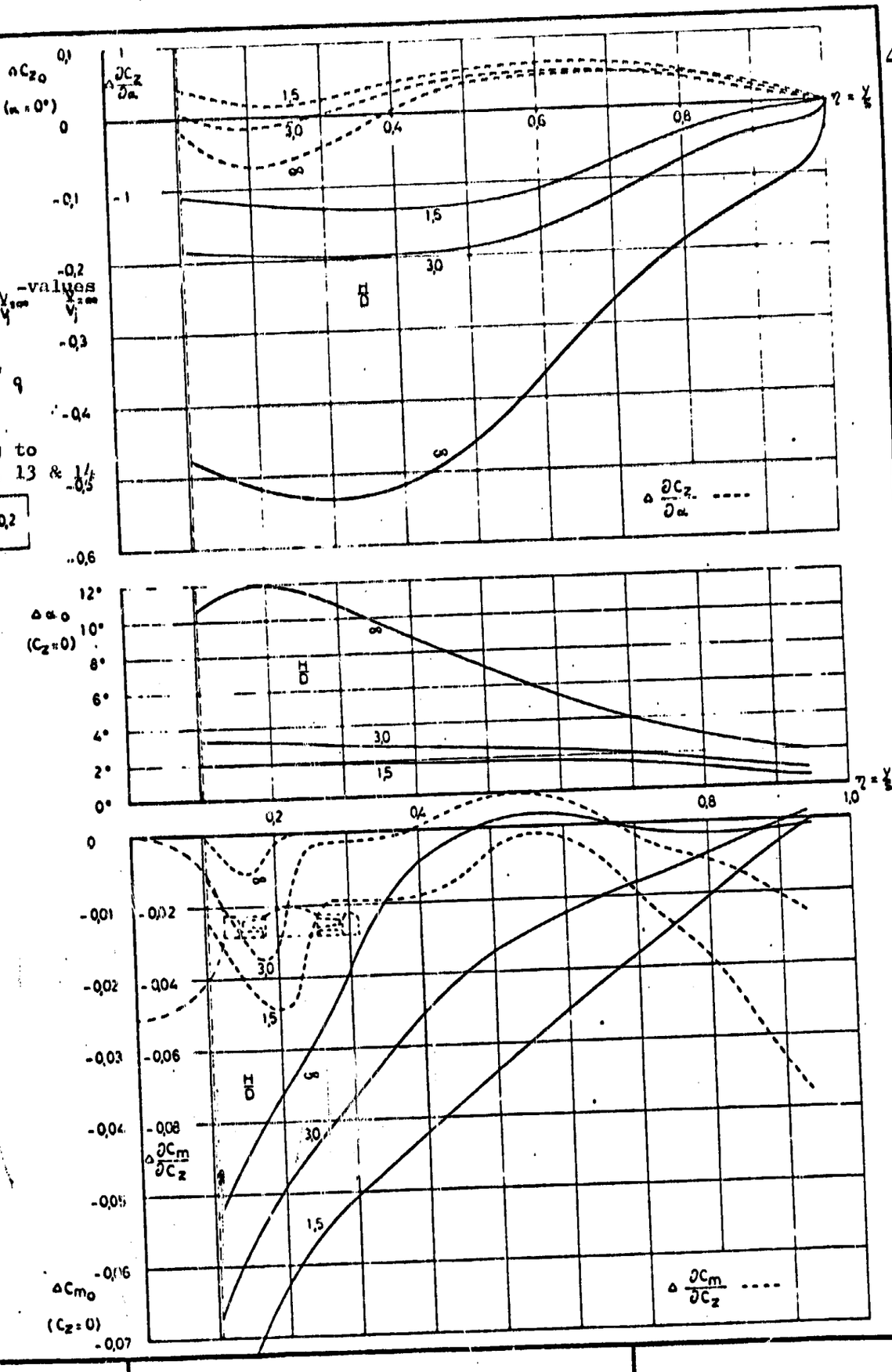

[Commas represent decimal points].

Fig. 15 — Pressure measurements Config. A

$\Delta C_{z_0}; \Delta \frac{\partial C_z}{\partial \alpha}; \Delta \alpha_0; \Delta C_{m_0}; \Delta \frac{\partial C_m}{\partial C_z} = f(\eta); \frac{H}{D} = \infty; 3,0; 1,5$

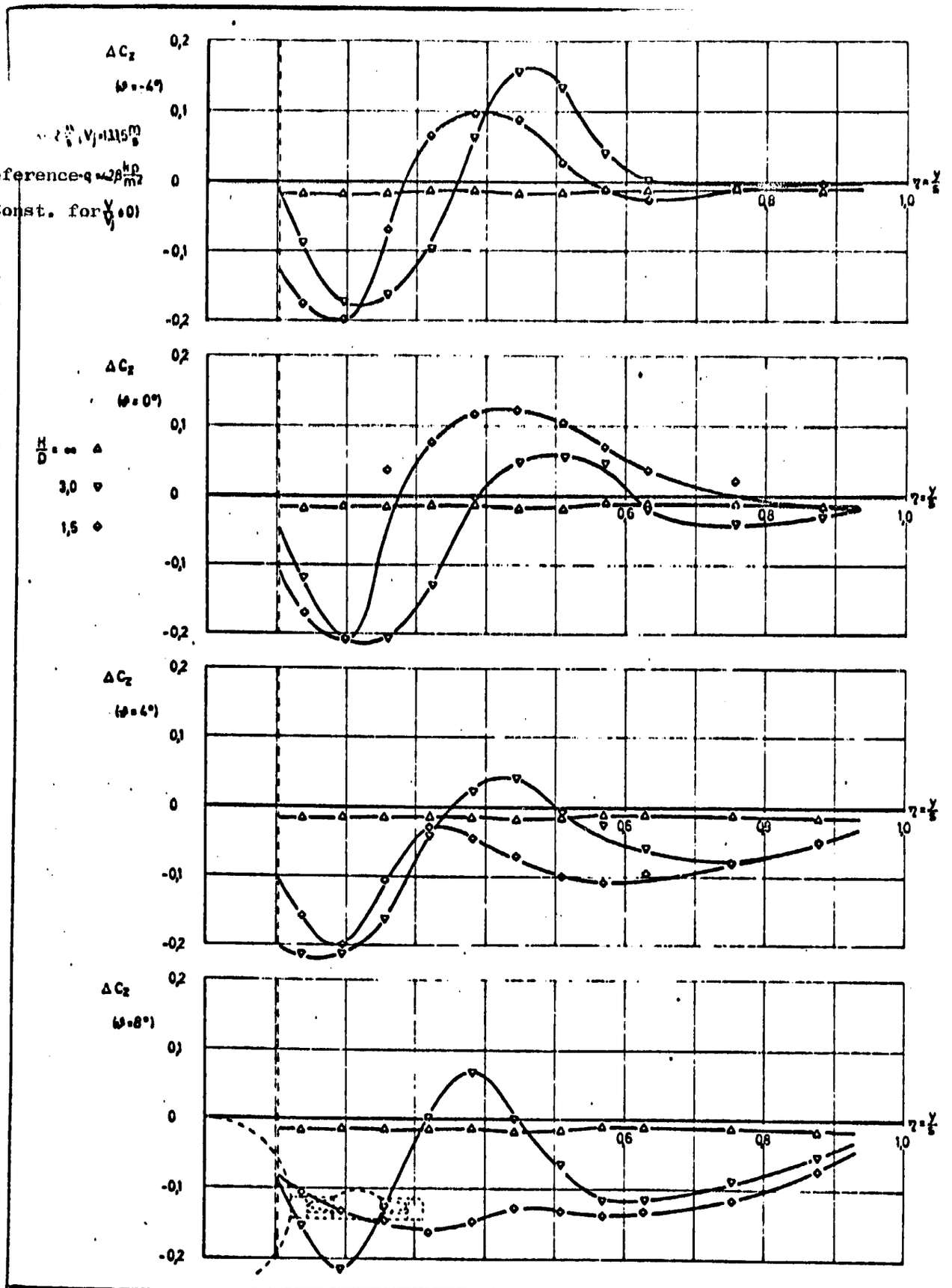

[Commas represent decimal points].

Fig. 16

Pressure measurements Config. A

$\Delta C_z = f(\eta)$ for $\frac{H}{D} = \infty ; 3,0 ; 1,5$

HF B

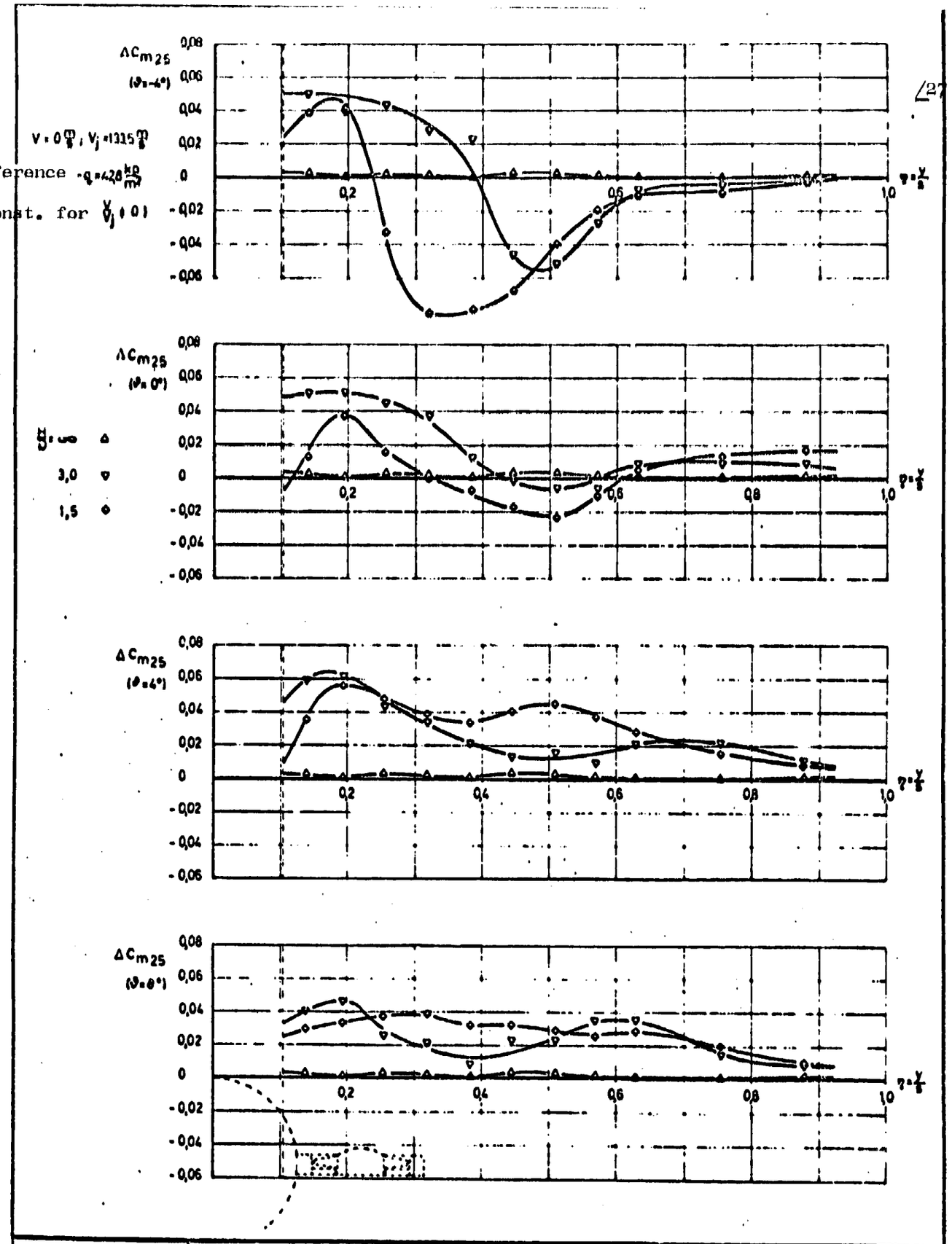

[Commas represent decimal points]

Fig. 17	Pressure measurements Config. A $\Delta C_{m25} = f(\eta)$ for $\frac{H}{D} = \infty; 3,0; 1,5$	HFB 31

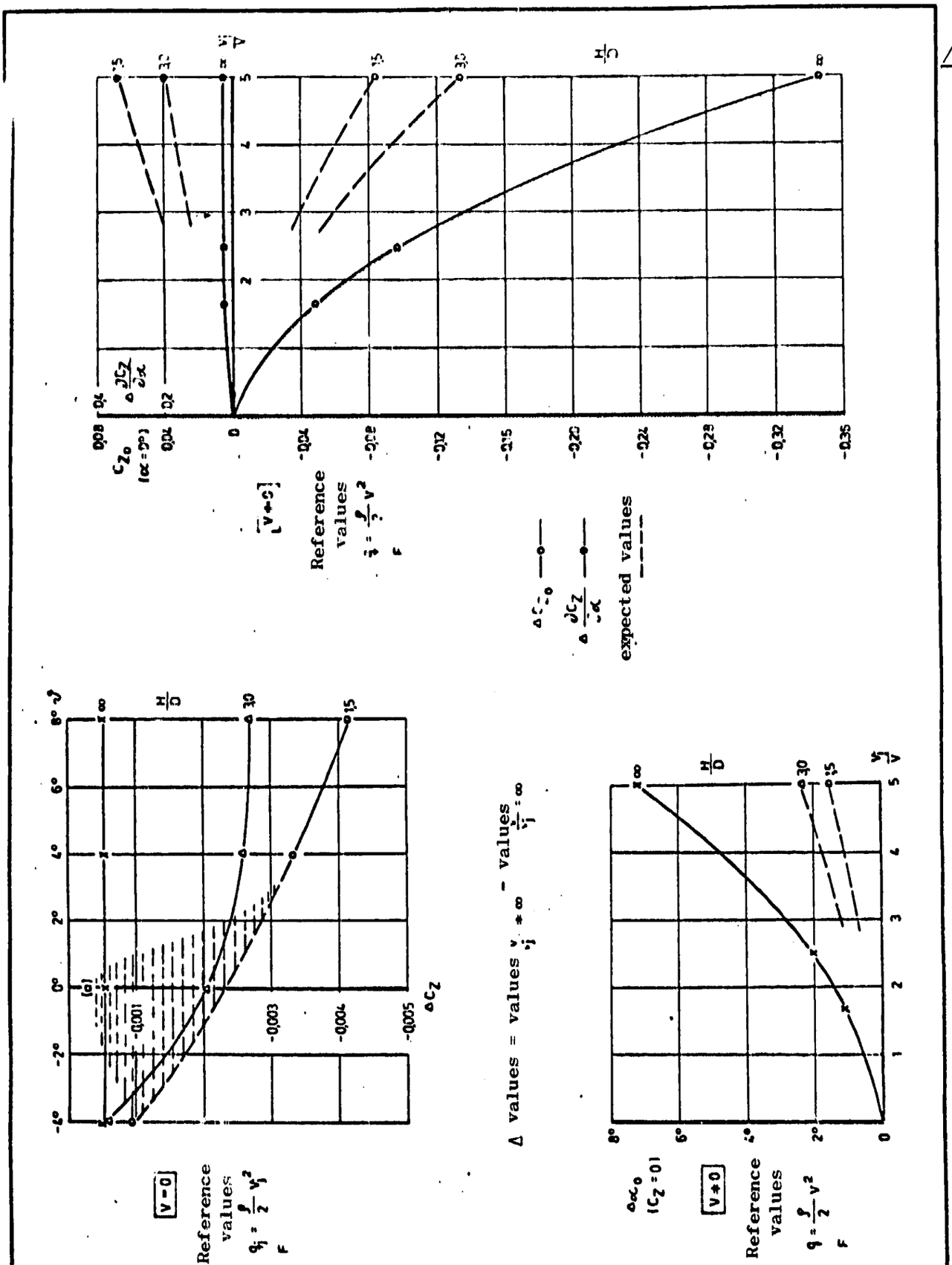

[Commas represent decimal points]

Fig. 18 — Integrations for entire wing Config. A — Normal force coefficients — HFB

Fig. 19

Integrations for entire wing Config. A

Rolling-moment coefficients

HFB

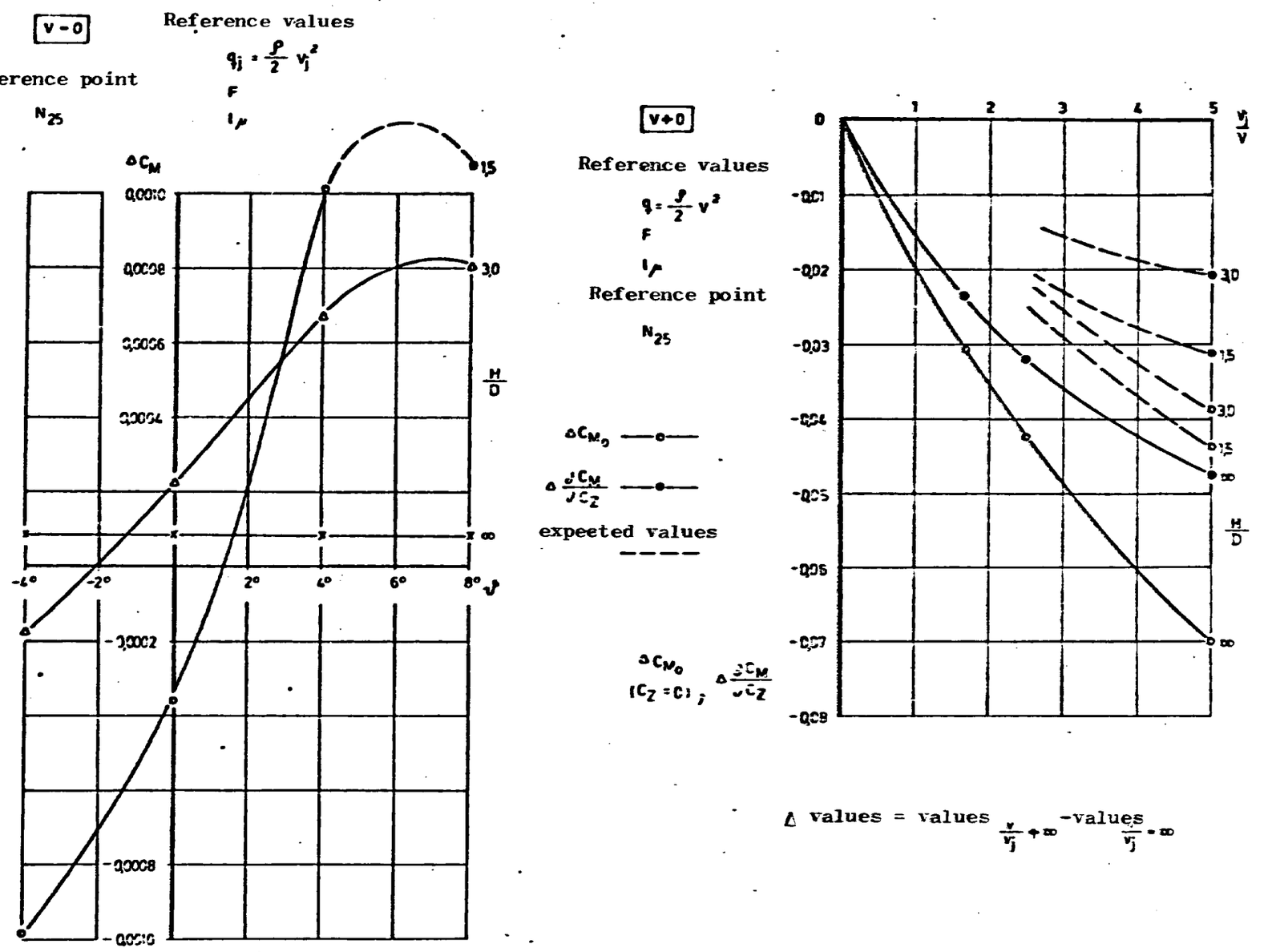

Δ values = values $_{\frac{v}{v_j} \neq \infty}$ -values $_{\frac{v}{v_j} = \infty}$

[Commas represent decimal points]

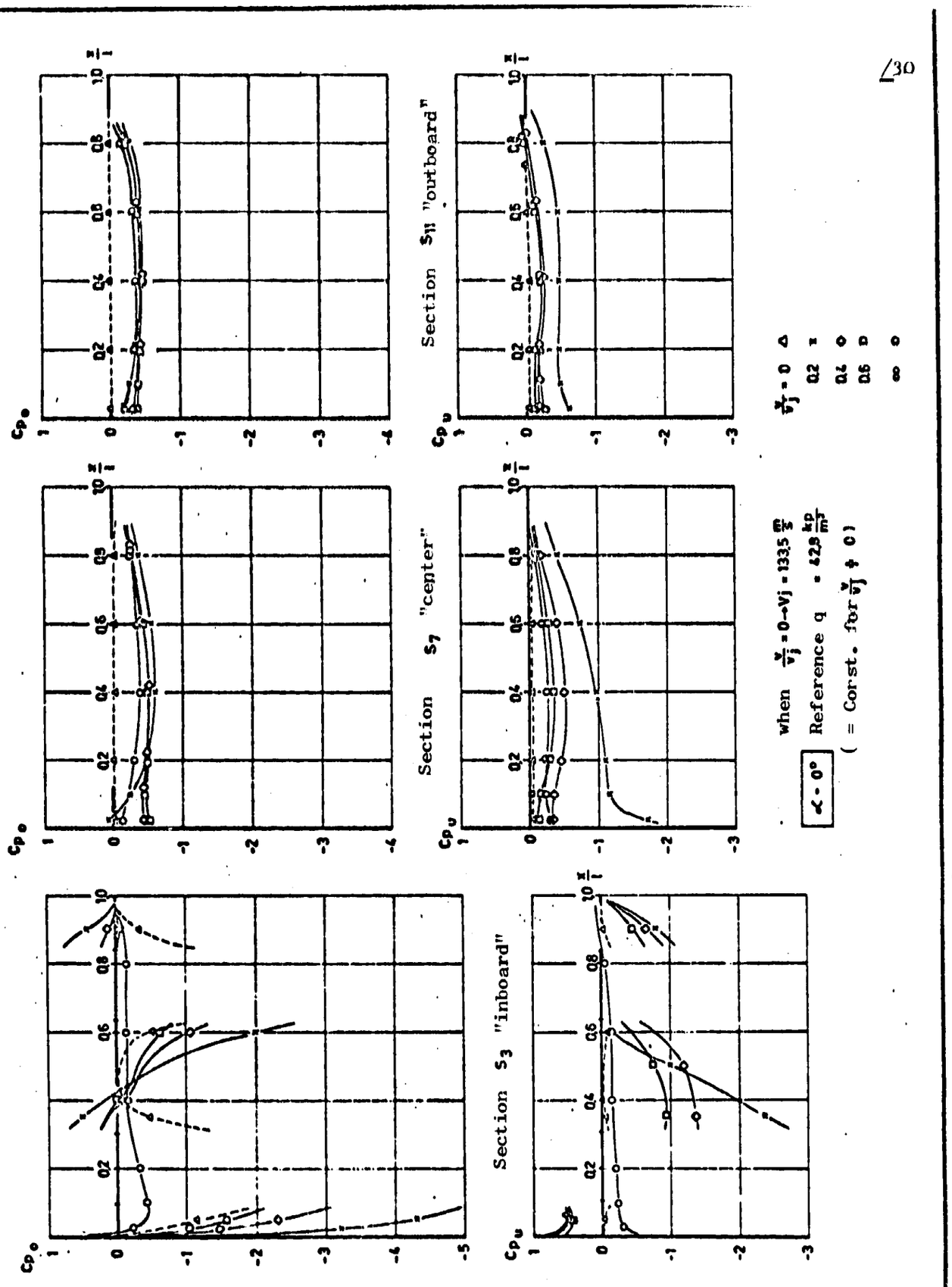

/30

Fig. 20 — Pressure measurements Config. B

$C_p = f\left(\frac{x}{l}\right)$ for $\frac{H}{D} = \infty$

HFB

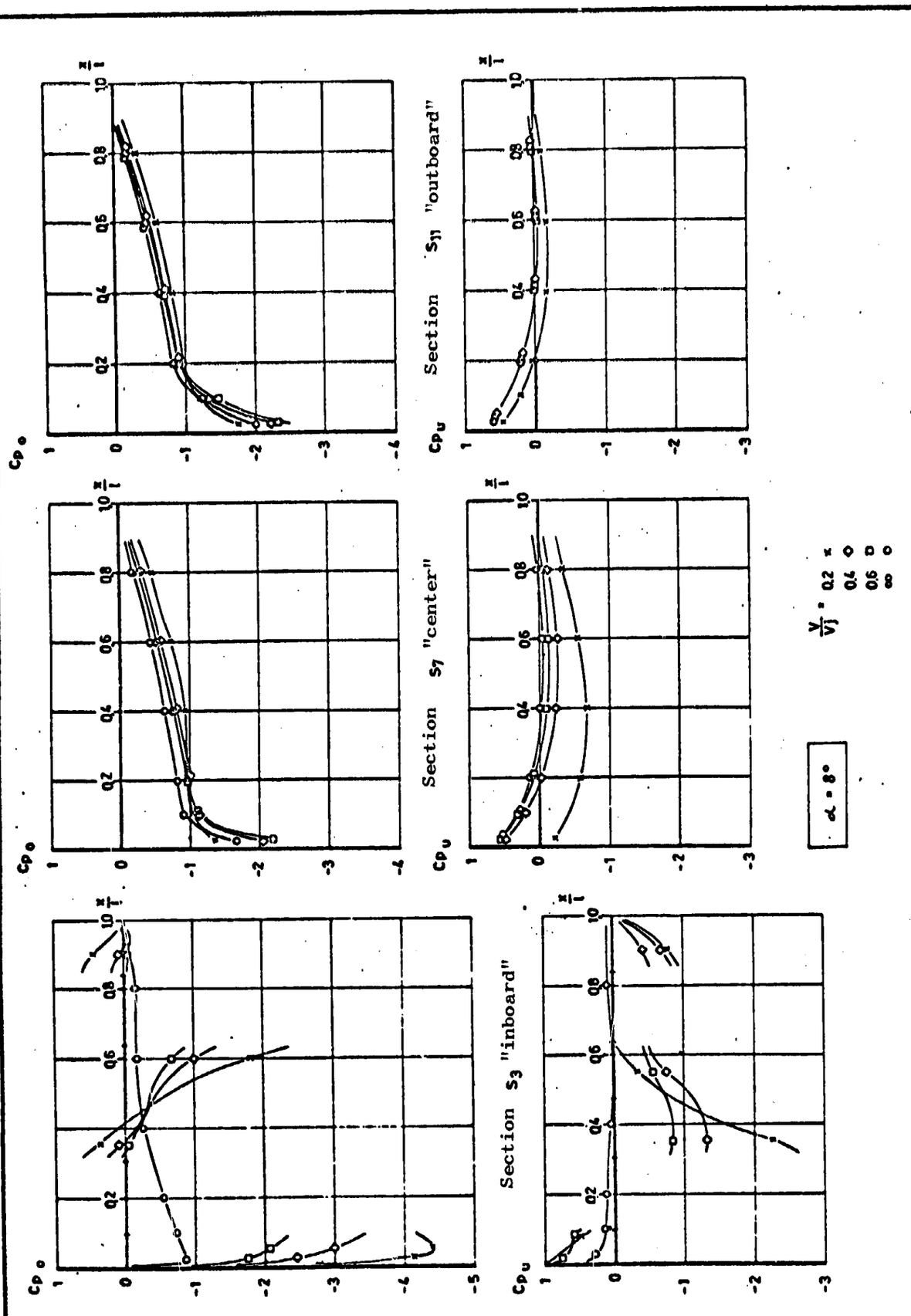

Fig. 21

Pressure measurements Config. B

$C_p = f\left(\frac{x}{l}\right)$ for $\frac{H}{D} = \infty$

HFB

[Commas represent decimal points]

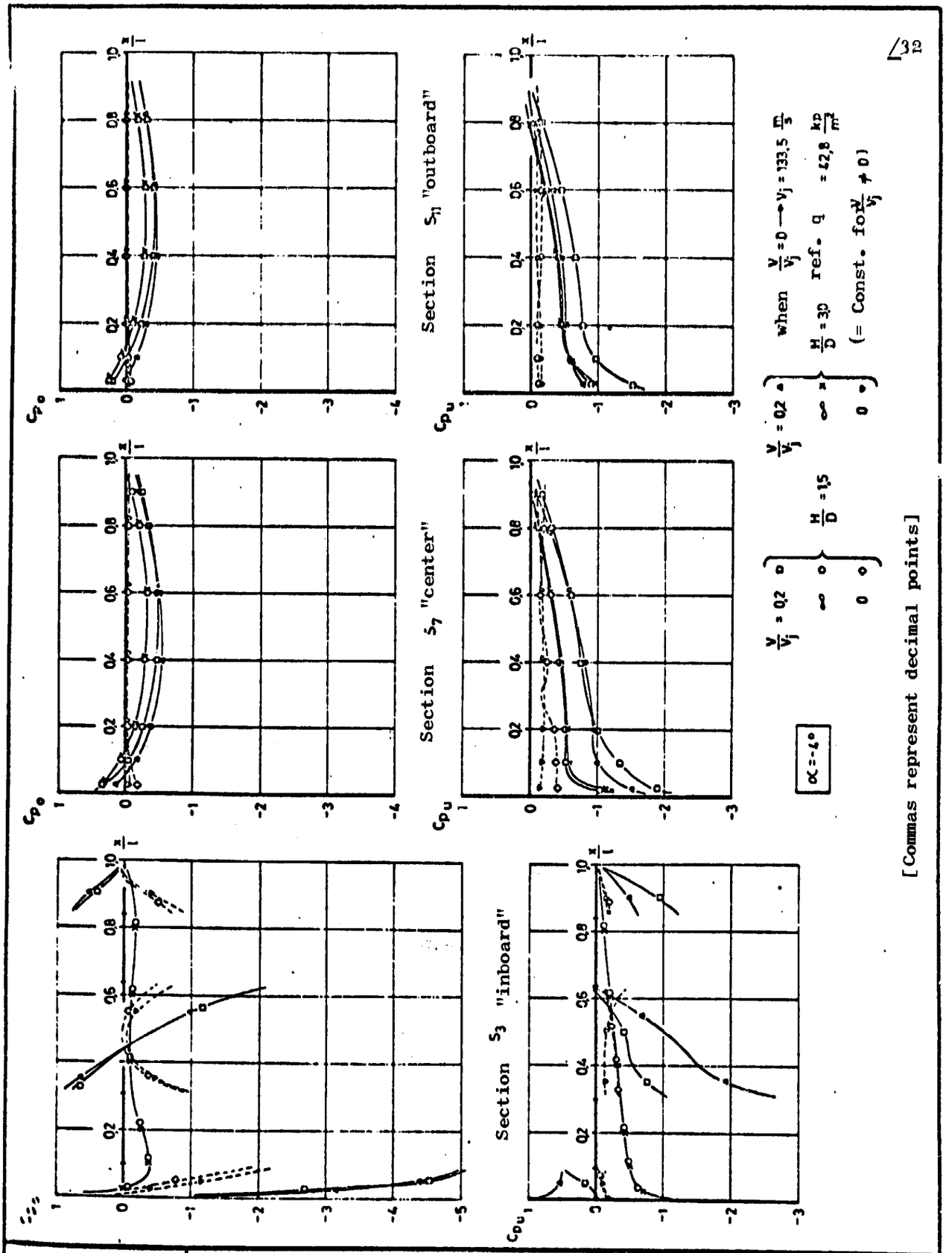

Fig. 22 — Pressure measurements Config. B
$C_p = f\left(\frac{x}{l}\right)$ for $\frac{H}{D}$ = 3,0 ; 1,5

HFB

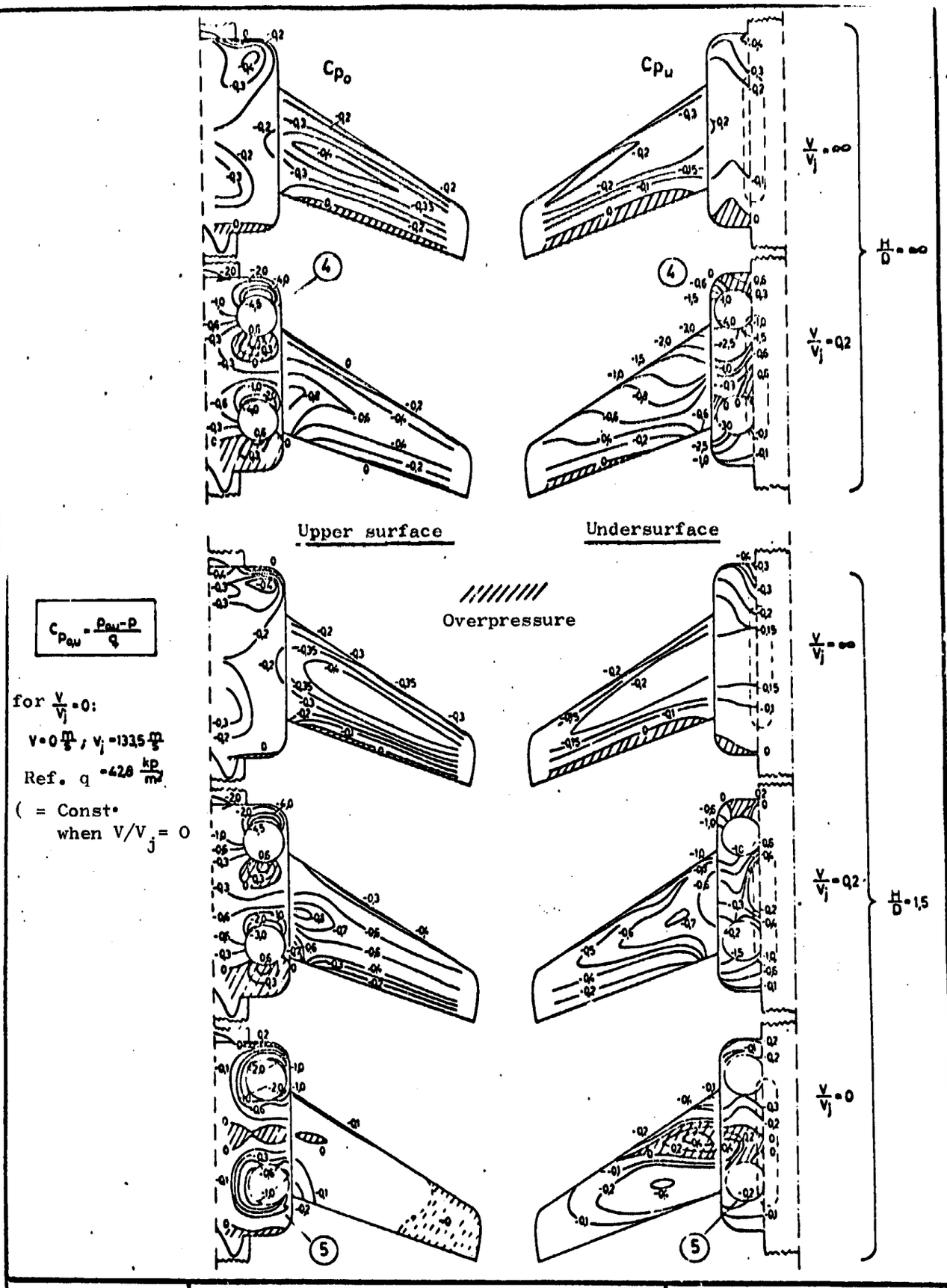

$C_{p_{o,u}} = \frac{p_{o,u} - p}{q}$

for $\frac{V}{V_j} = 0$:

$V = 0 \frac{m}{s}$; $V_j = 133.5 \frac{m}{s}$

Ref. q $42.8 \frac{kp}{m^2}$

(= Const. when $V/V_j = 0$

∠33

[Commas represent decimal points]

Fig. 23	Pressure measurement Config. B . Isobar distribution for α or $\vartheta = 0°$	HFB	37

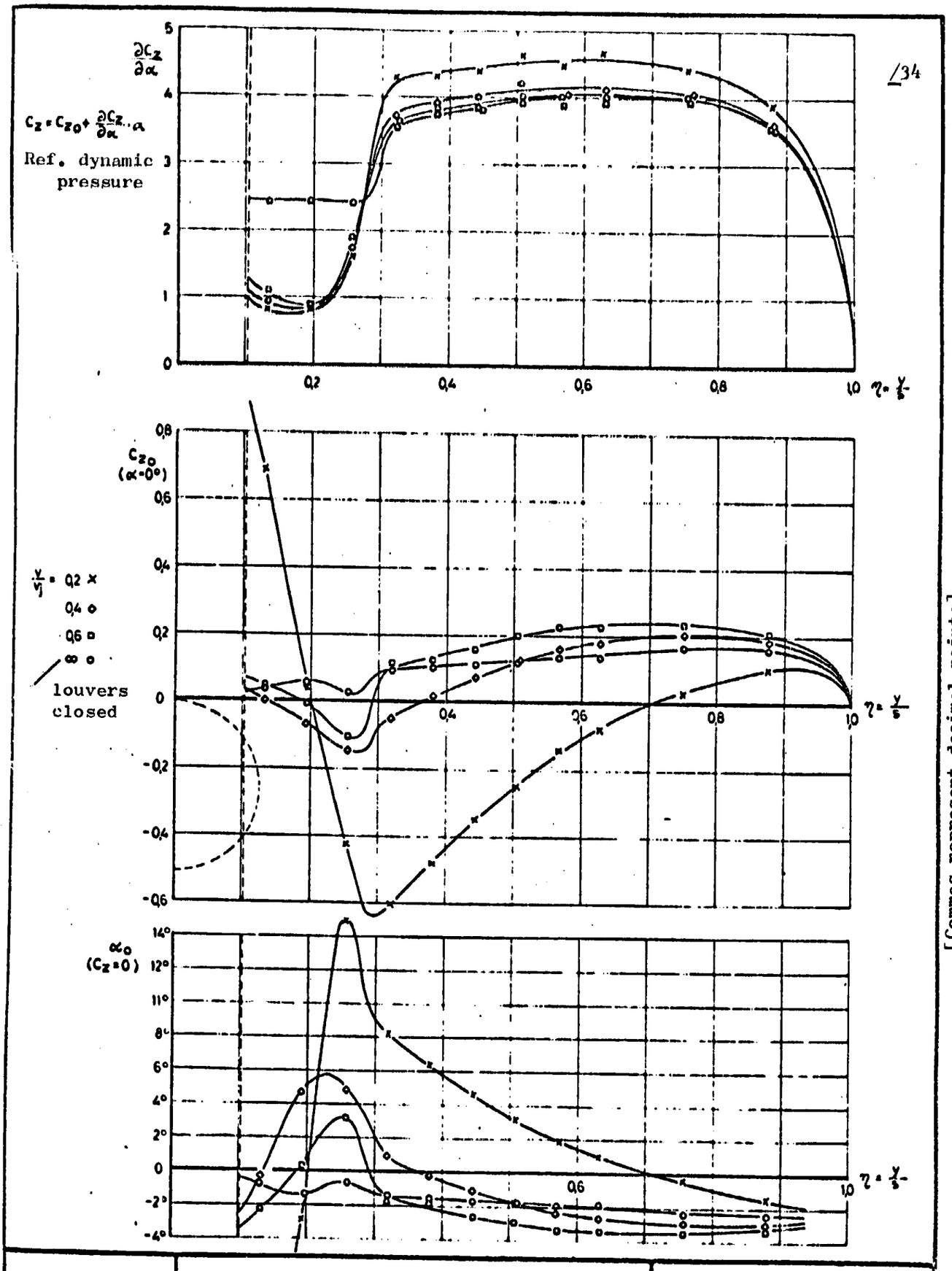

/34

[Commas represent decimal points]

38	Fig. 24	Pressure measurement Config. B $\frac{\partial C_z}{\partial \alpha}$; C_{z0} ; α_0 = f(η) for $\frac{H}{D} = \infty$	HFB

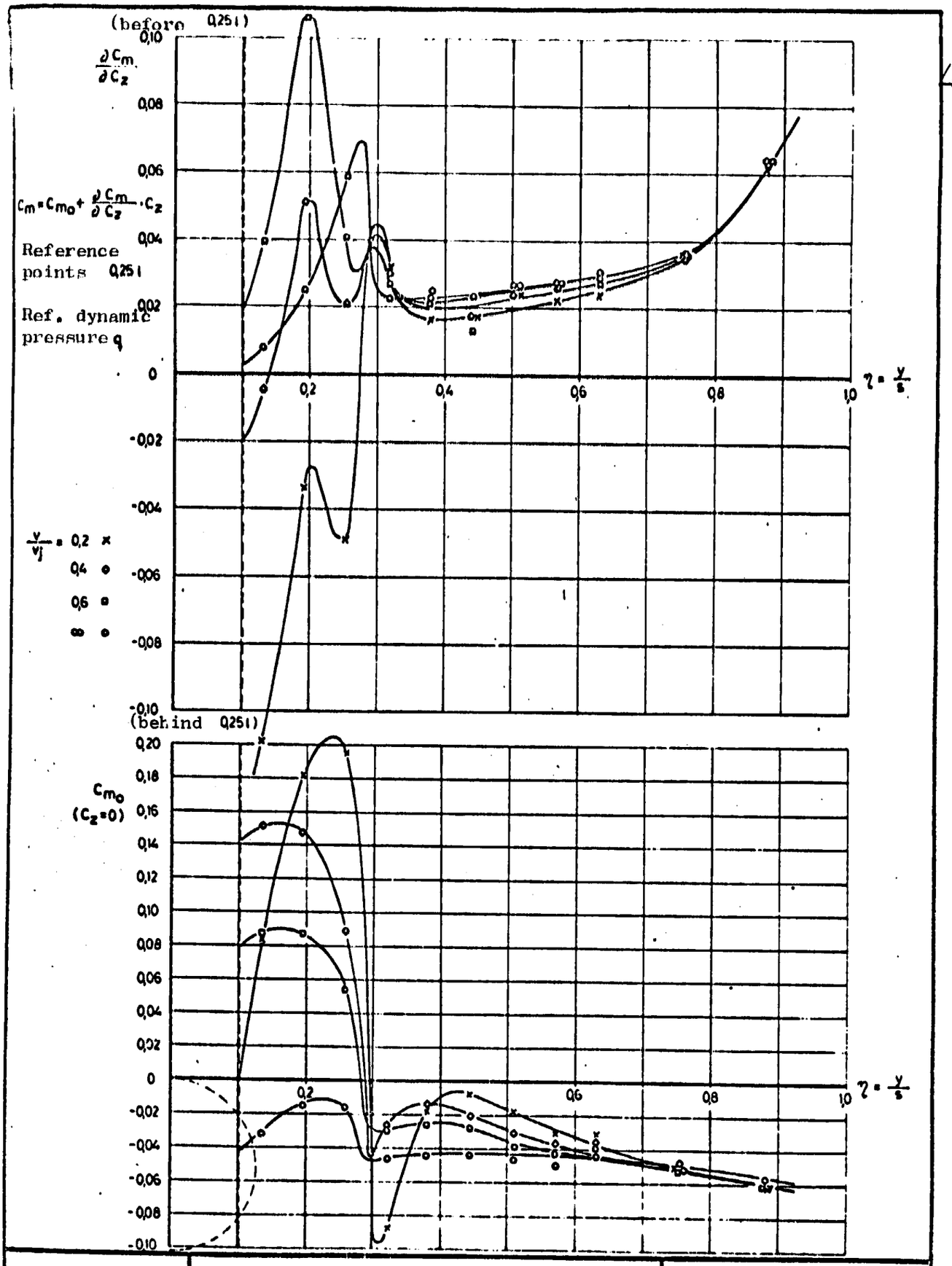

Fig. 25

Pressure measurement Config. B

$\frac{\partial C_m}{\partial C_z}$, $C_{m_o} = f(\eta)$ for $\frac{H}{D} = \infty$

HFB

[Commas represent decimal points]

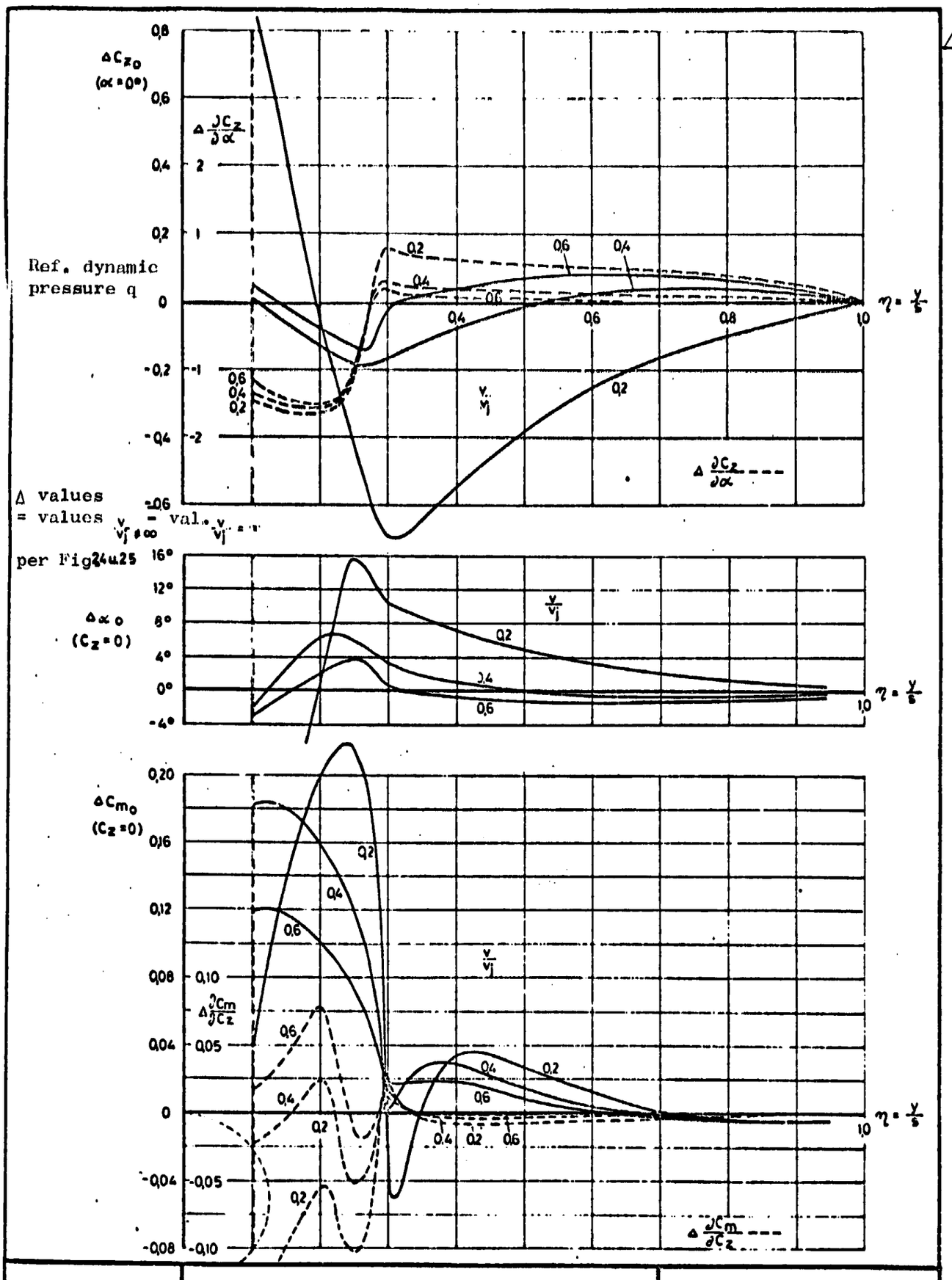

[Commas represent decimal points]

40	Fig. 26	Pressure measurement Config. B $\Delta C_{z0}; \Delta\frac{\partial C_z}{\partial \alpha}; \Delta\alpha_0; \Delta C_{m0}; \Delta\frac{\partial C_m}{\partial C_z} = f(\eta)$ for $\frac{H}{D} = \infty$	HFB

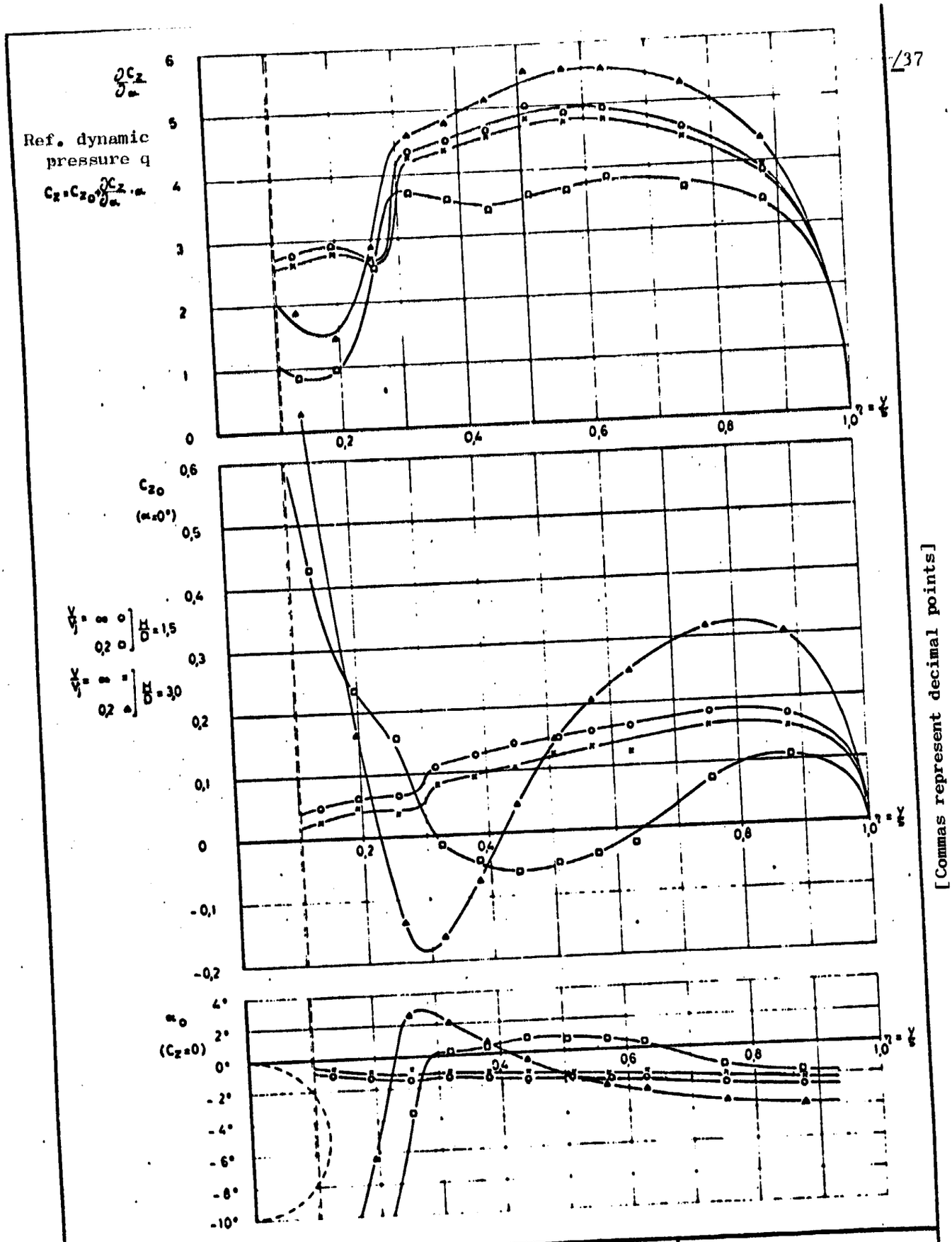
$\frac{\partial C_z}{\partial \alpha}$
Ref. dynamic pressure q
$C_z = C_{z_0} + \frac{\partial C_z}{\partial \alpha} \cdot \alpha$
C_{z_0} ($\alpha = 0°$)
$\frac{V}{V_\infty}$ = ∞ ○ 0,2 □ $\frac{H}{D}$ = 1,5
$\frac{V}{V_\infty}$ = ∞ × 0,2 △ $\frac{H}{D}$ = 3,0
α_0 ($C_z = 0$)
$\frac{V}{V_\infty}$

[Commas represent decimal points]

Fig. 27	Pressure measurements Config. B $\frac{\partial C_z}{\partial \alpha}$; C_{z_0}; $\alpha_0 = f(?)$ for $\frac{H}{D}$ = 3,0 ; 1,5	HFB

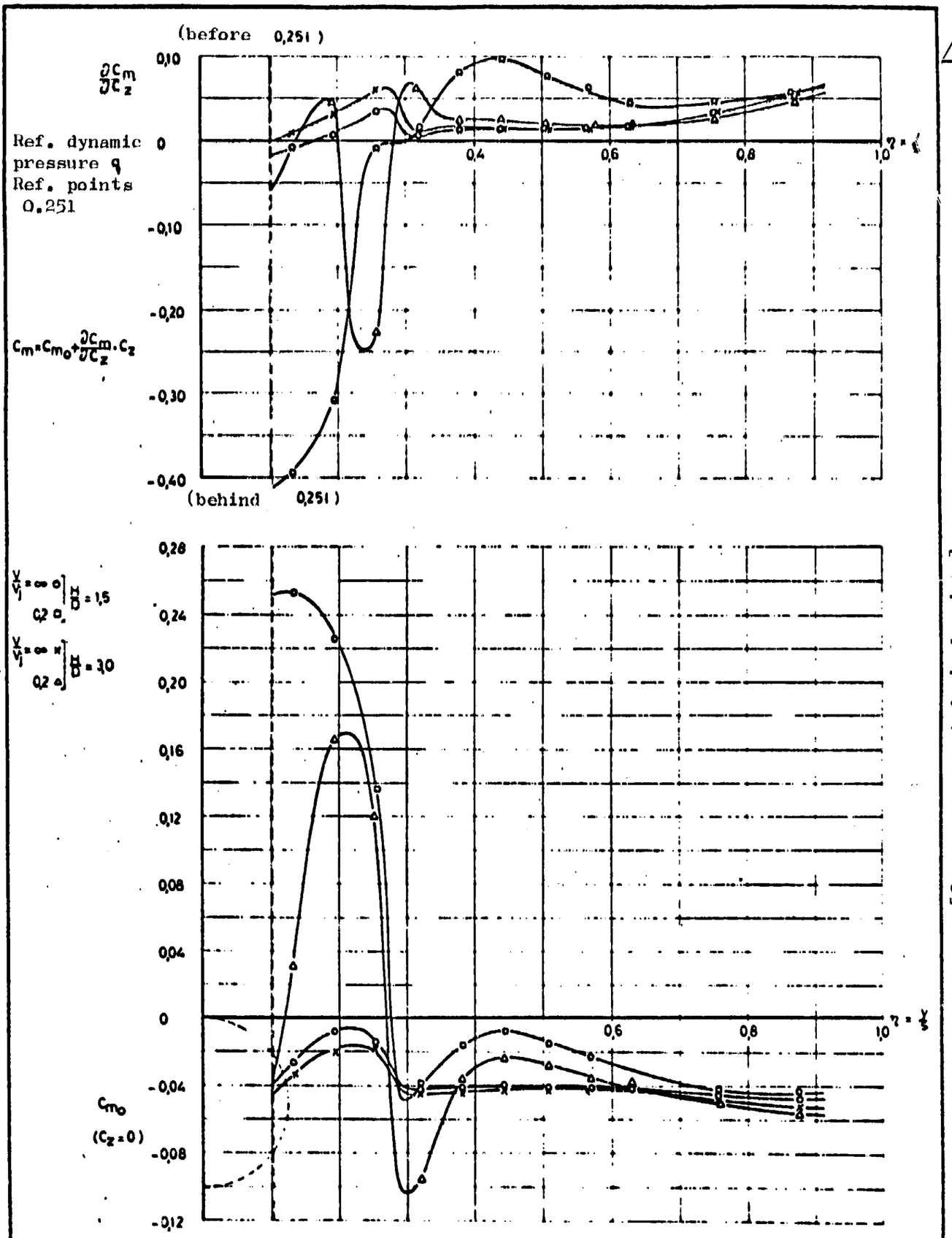

[Commas represent decimal points]

Fig. 28	Pressure measurements Config. B $\frac{\partial C_m}{\partial C_z}$, $C_{m_0} = f(\eta)$ for $\frac{H}{D} = 3,0; 1,5$	HFB

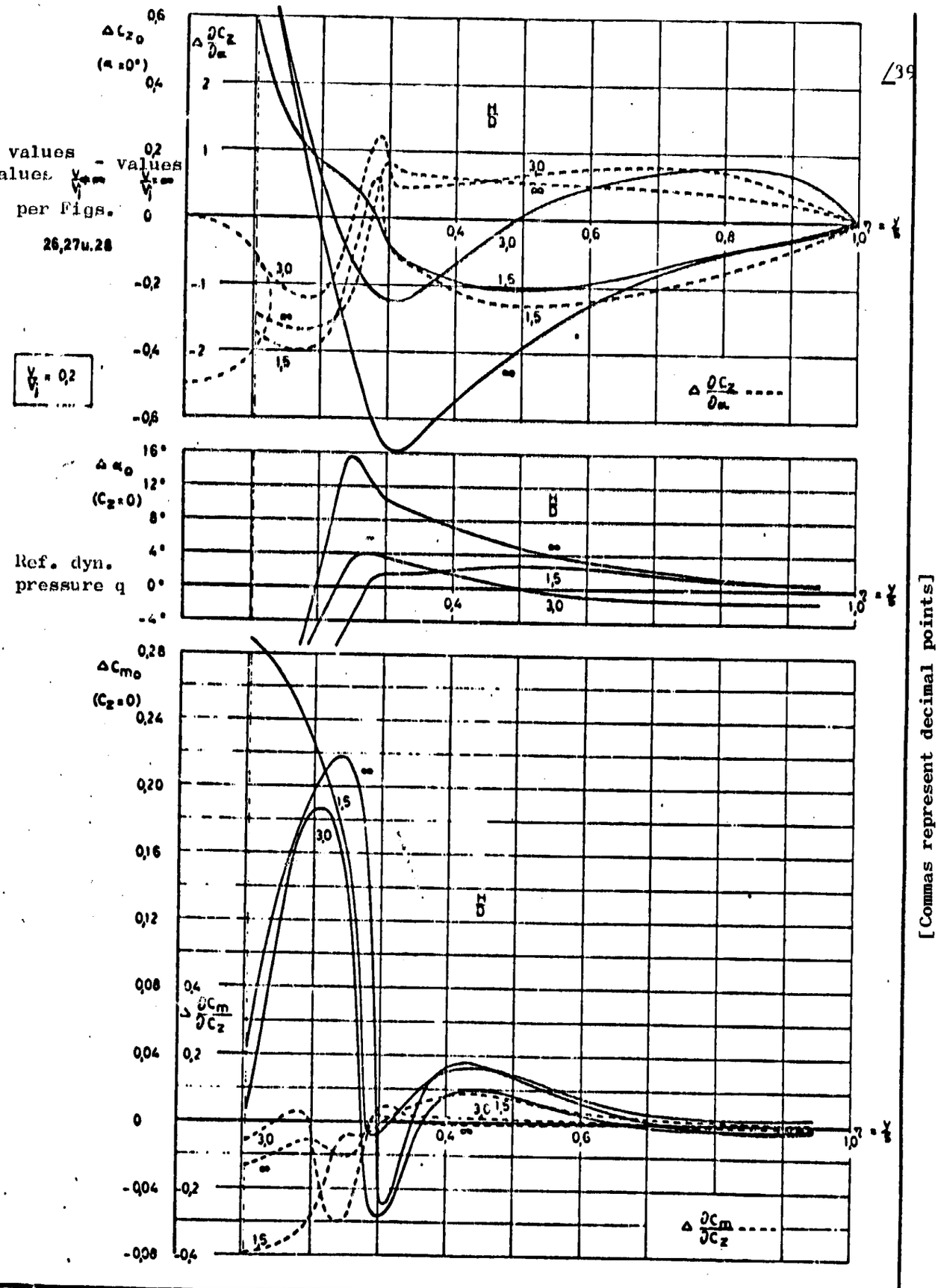
Δ values = values − values per Figs. 26,27u.28
$\frac{V}{V_i} = 0{,}2$
ΔC_{z_0} ($\alpha = 0°$)
$\Delta \frac{\partial C_z}{\partial \alpha}$
$\Delta \alpha_0$ ($C_z = 0$)
ΔC_{m_0} ($C_z = 0$)
$\Delta \frac{\partial C_m}{\partial C_z}$
$\frac{H}{D}$
$\frac{V}{V_i}$
Ref. dyn. pressure q

[Commas represent decimal points]

Fig. 29	Pressure measurements Config. B $\Delta C_{z_0}, \Delta \frac{\partial C_z}{\partial \alpha}, \Delta \alpha_0, \Delta C_{m_0}, \Delta \frac{\partial C_m}{\partial C_z} = f(?) \text{ for } \frac{H}{D} = \infty, 3{,}0, 1{,}5$	HFB

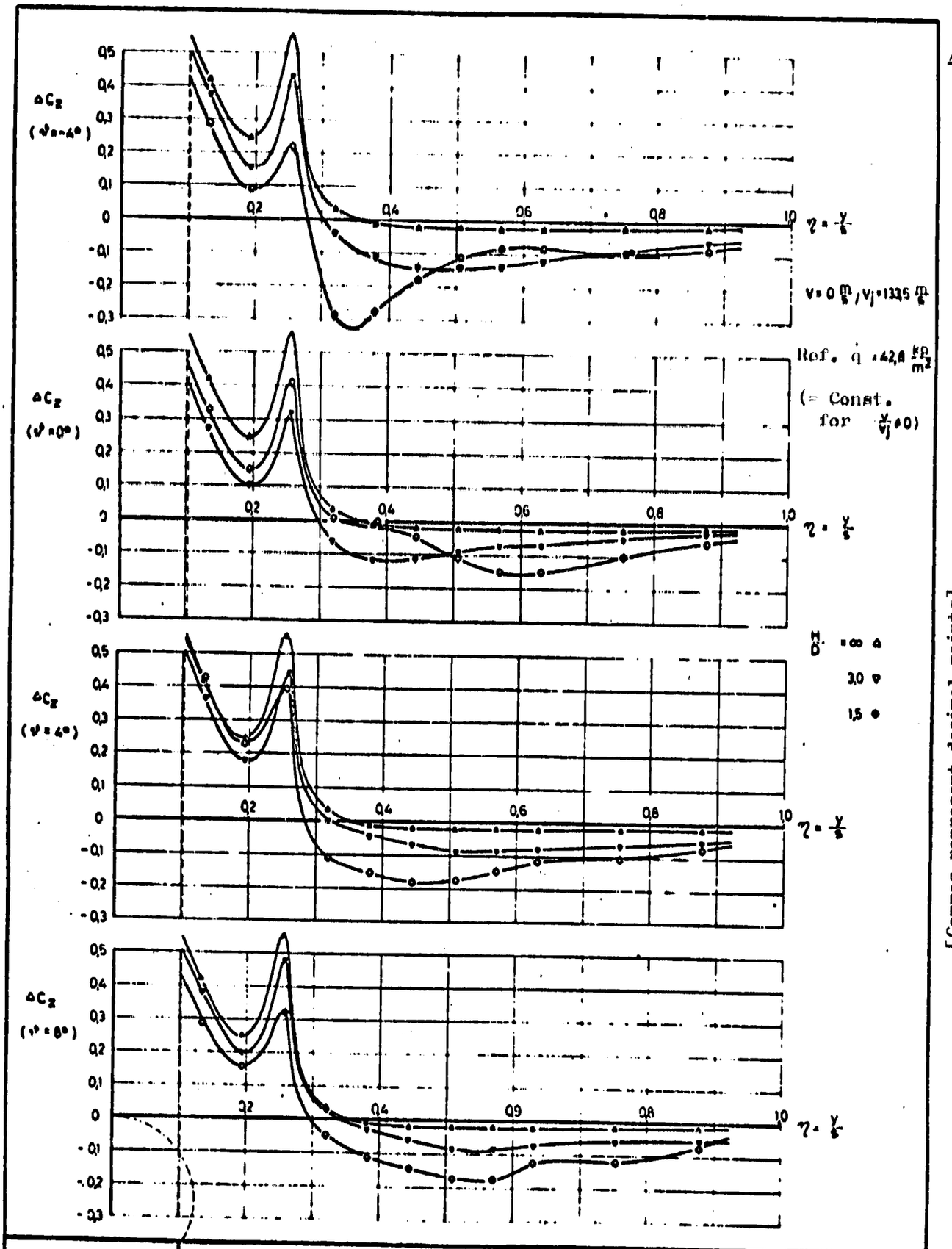

[Commas represent decimal points]

Fig. 30	Pressure measurements Config. B $\Delta C_z = f(\eta)$ for $\frac{H}{D} = \infty, 3,0, 1,5, V = 0$	HFB

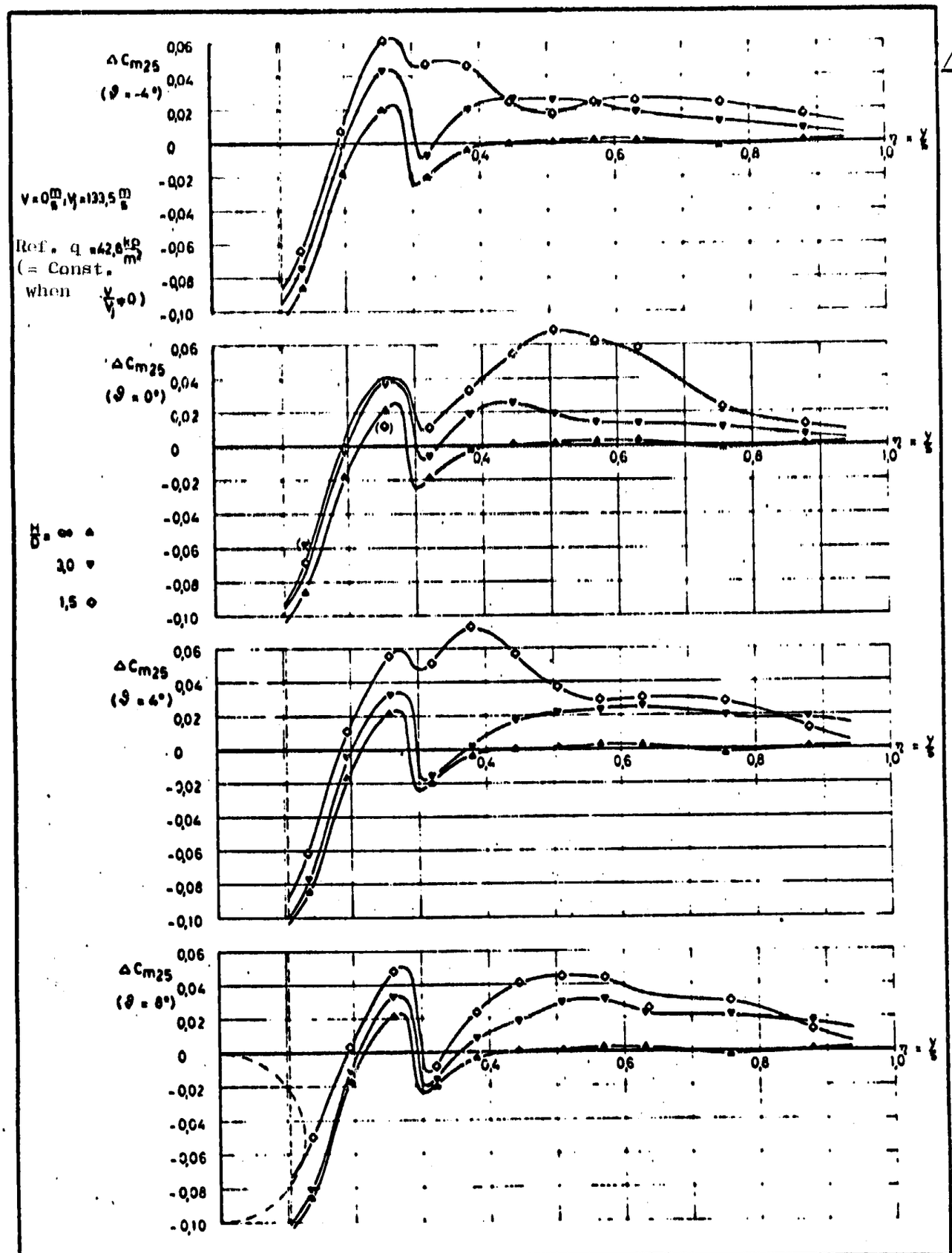

[Commas represent decimal points]

Fig. 31	Pressure measurements Config. B $\Delta C_m = f(\eta)$ for $\frac{H}{D} = \infty, 3.0, 1.5, V=0$	HFB 45

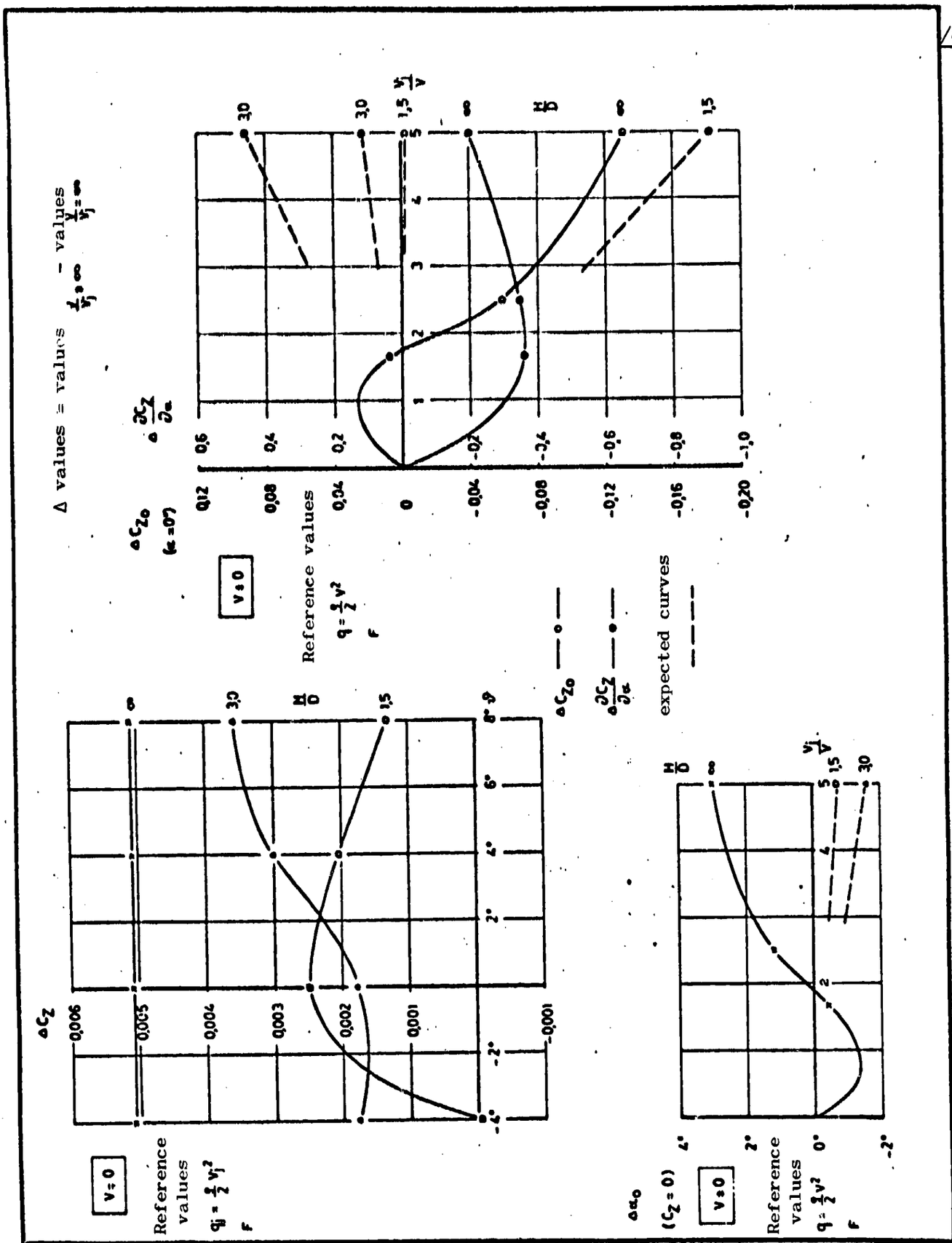

Fig. 32 Integrations for entire wing Config. B

Normal force coefficients

HFB

Fig. 33

Integrations for entire wing

Config. B

Rolling-moment coefficients

HFB

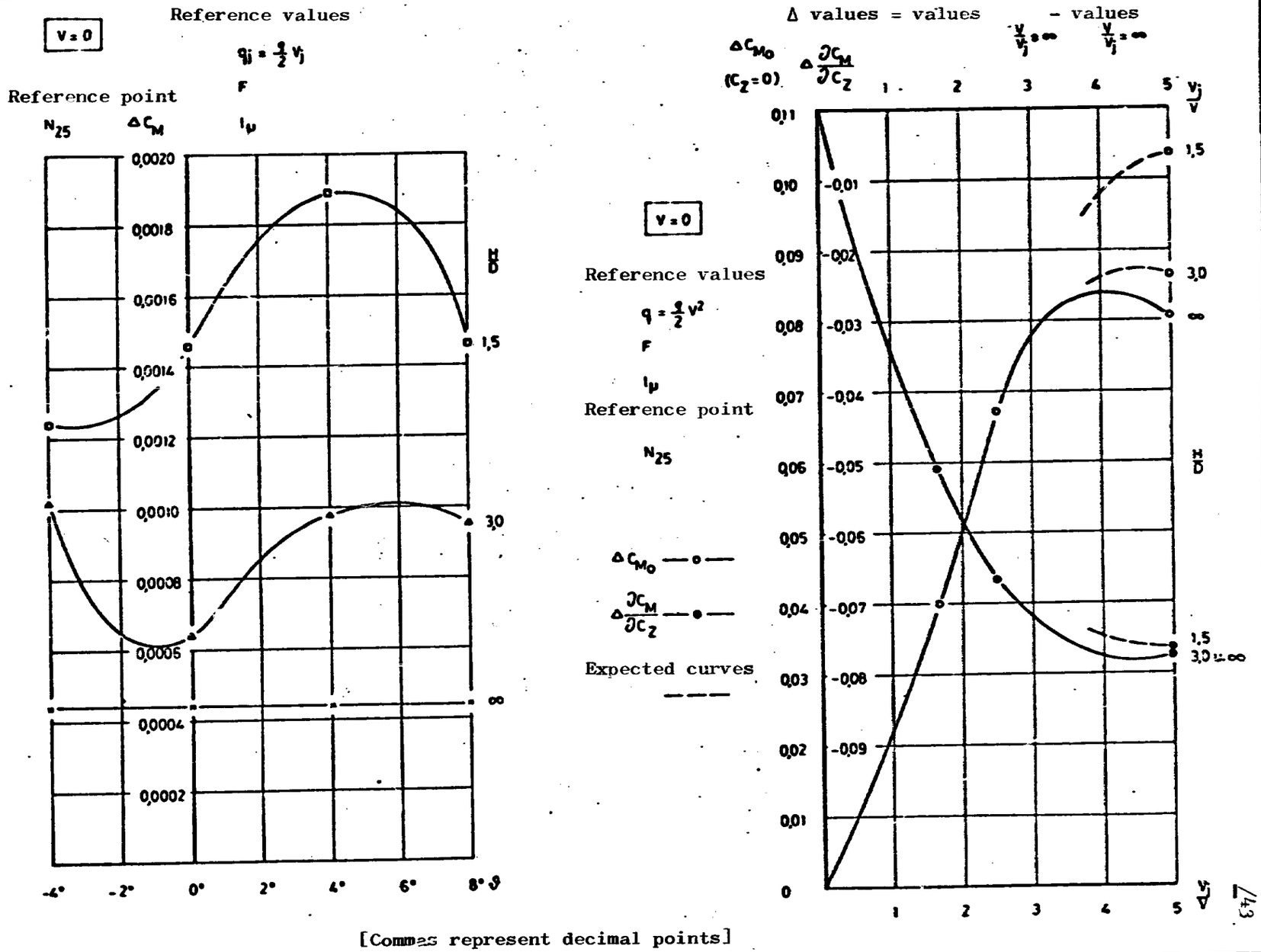

[Commas represent decimal points]

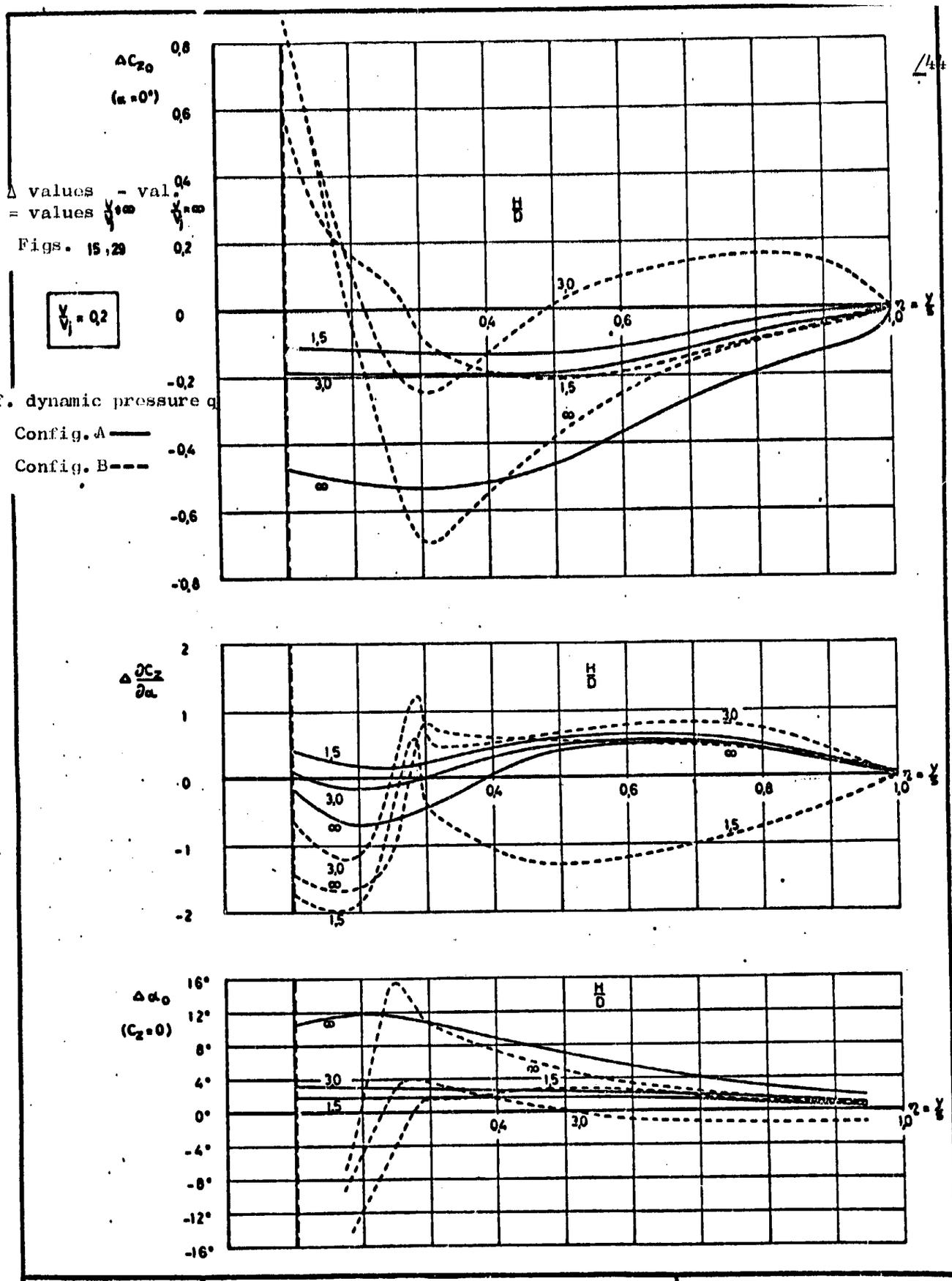

48	Fig. 34	Characteristic differences Normal force coefs. $V \neq 0$ Configs. A & B	HFB

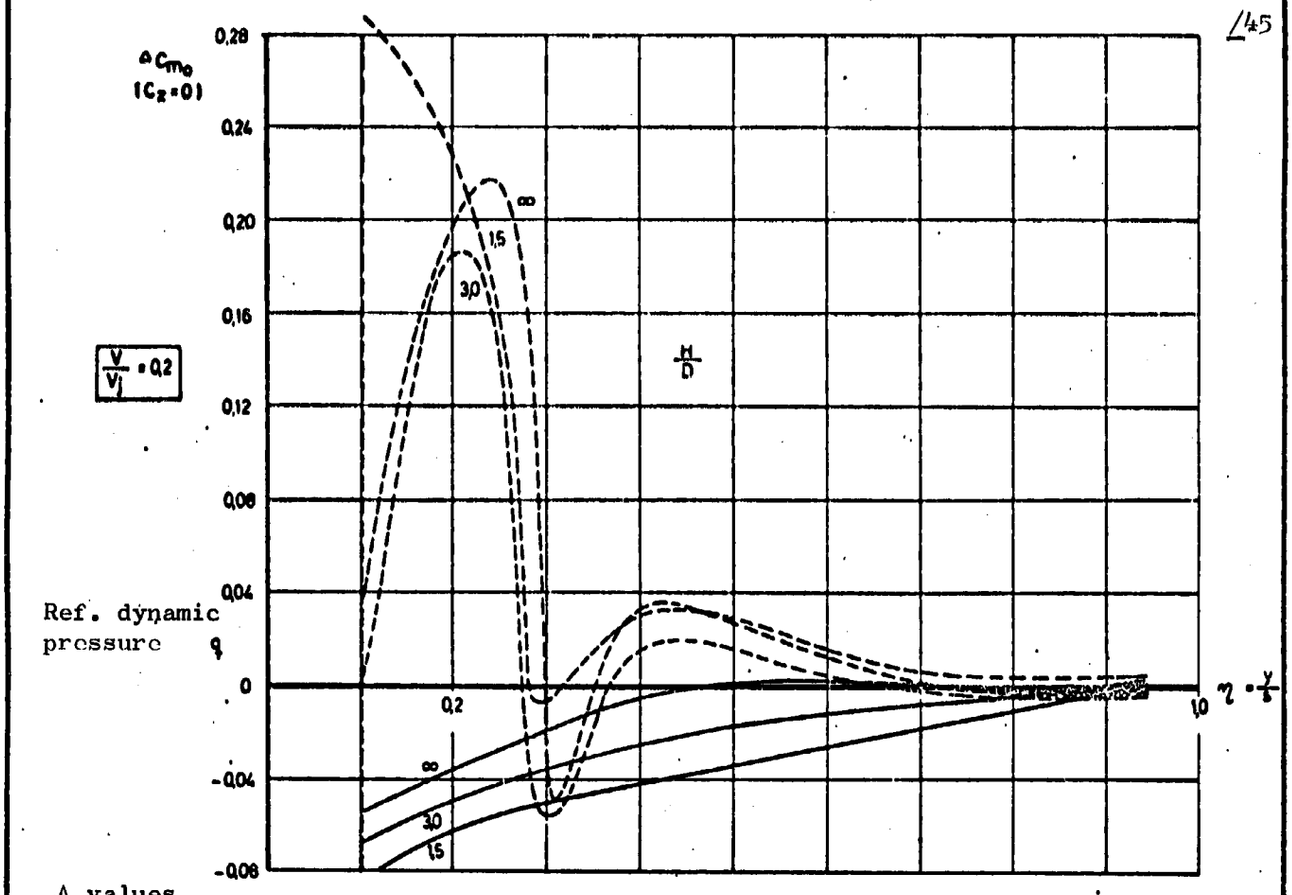

Δ values = values $\frac{V}{V_j} \neq \infty$ - val. $\frac{V}{V_j} = \infty$ per Figs. 15, 29

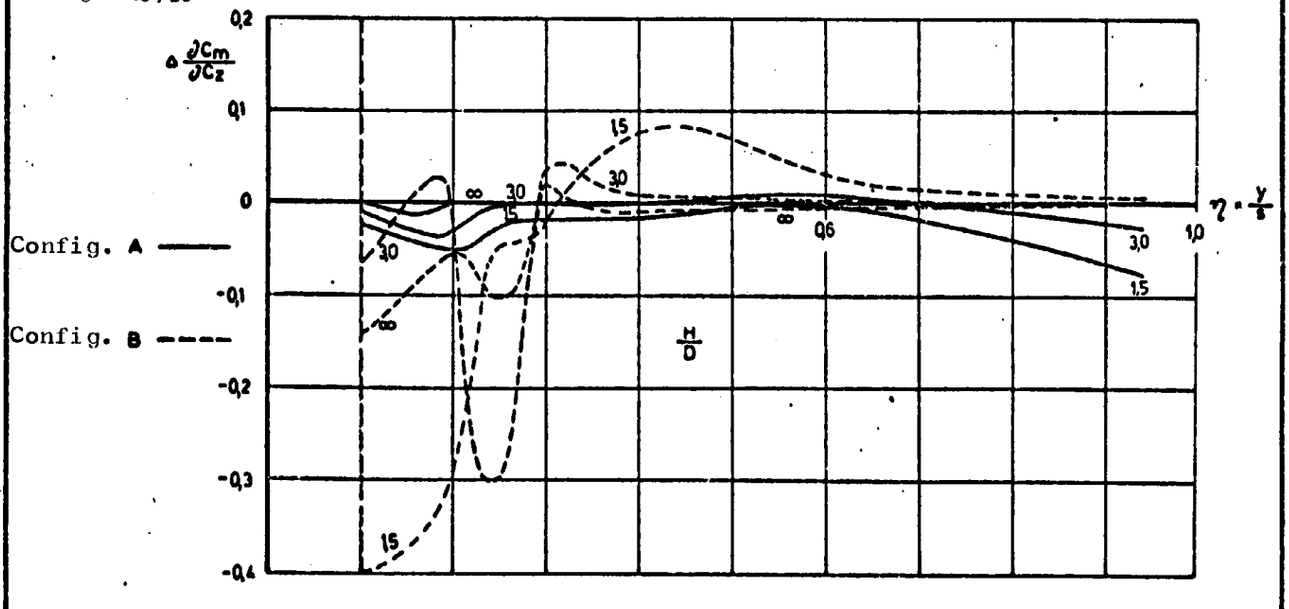

[Commas represent decimal points]

Fig. 35	Characteristic differences Rolling-moment coefs., V≠0	Configs. A & B	HFB 49

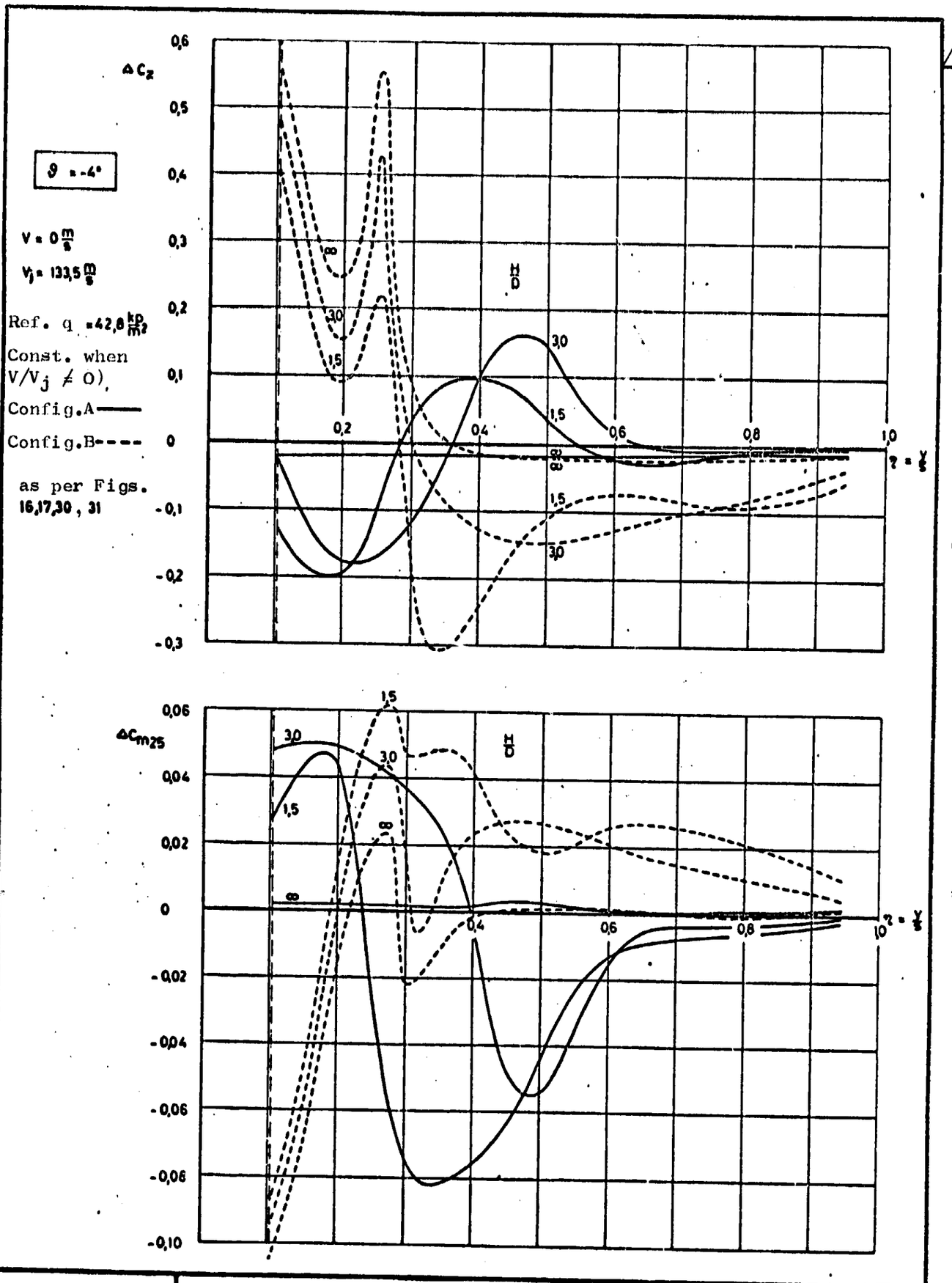

[Commas represent decimal points]

Fig. 36	Characteristic differences V=0	HFB

Config. A

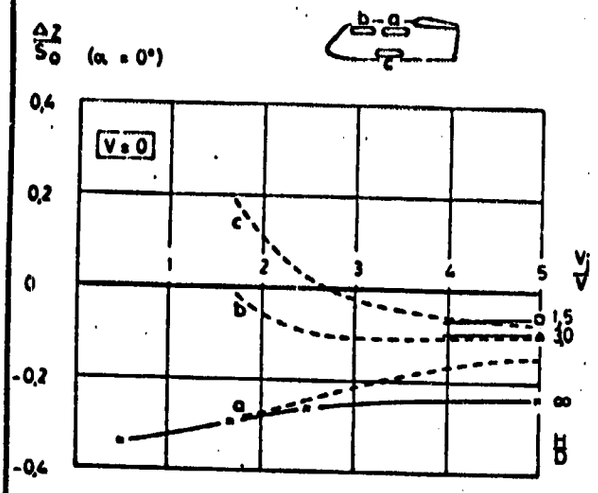

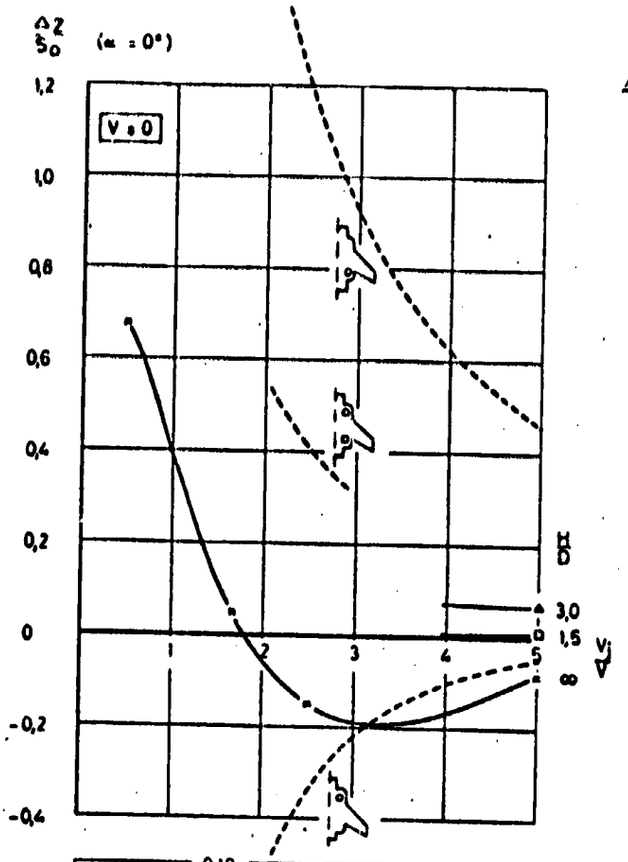

[Commas represent decimal points]

force measurements according to [2] when H/D = ∞

S_o for 4 engines according to Fig. 3

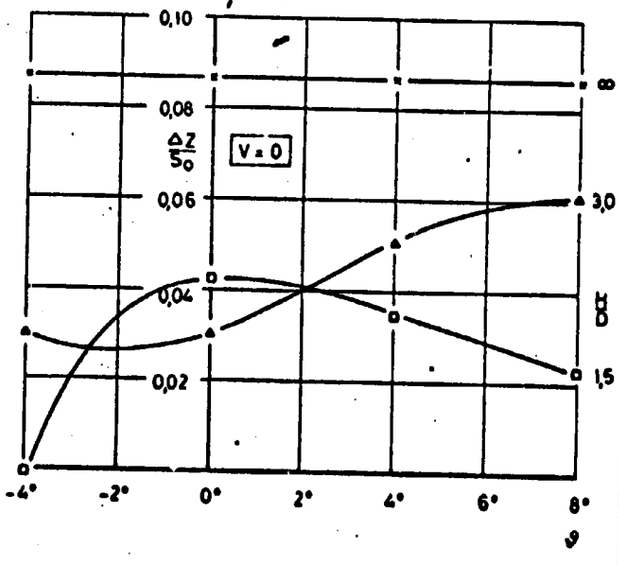

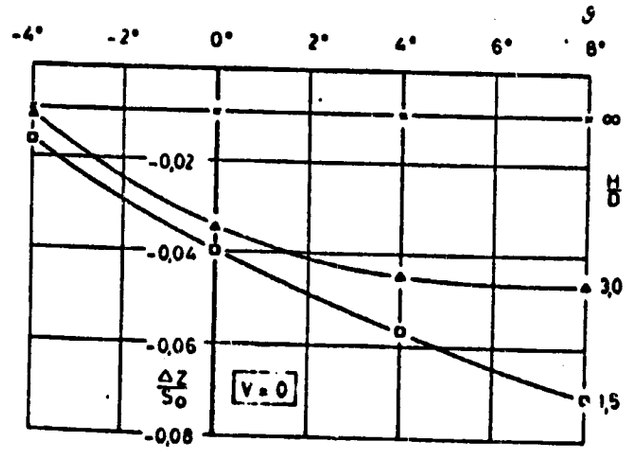

Config. B

Fig.37	Comparison $\frac{\Delta Z}{S_o}$ Configs. A & B with force measurements	HFB 51

Config. A

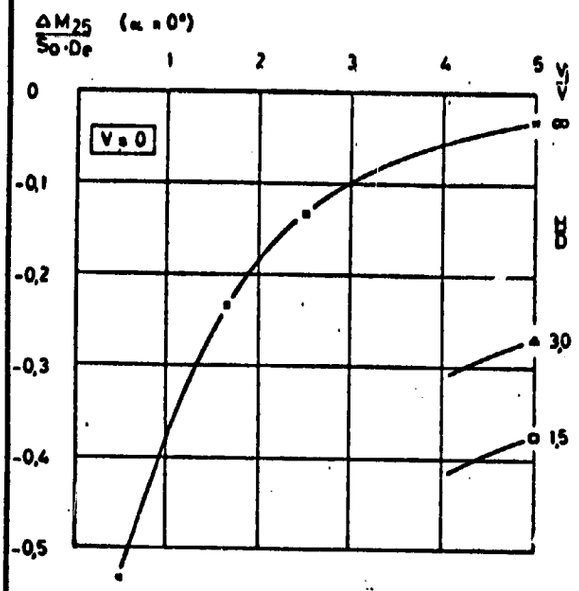

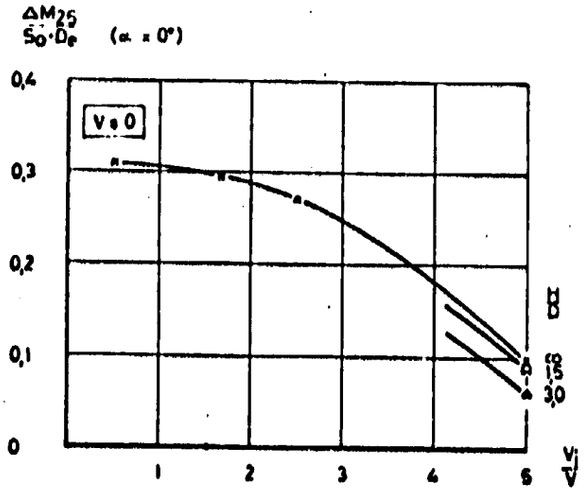

S_o for 4 engines according to Fig. 3

$D_e = \left(\frac{4 \Sigma F}{\pi}\right)^{1/2} = 0{,}294\,m$

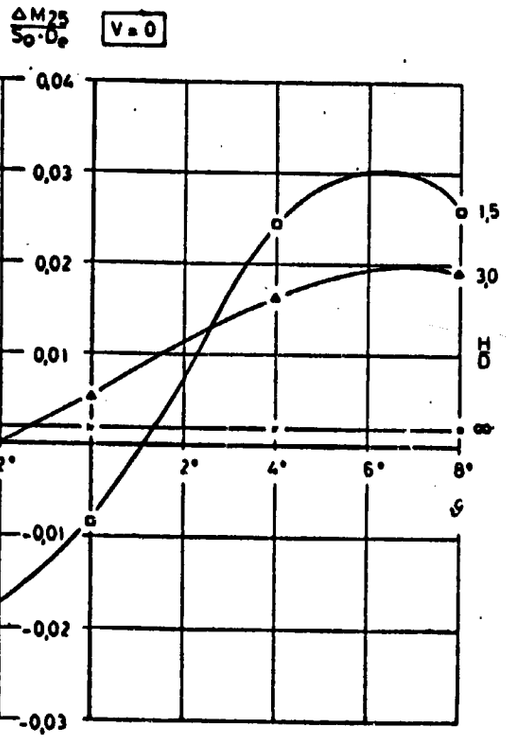

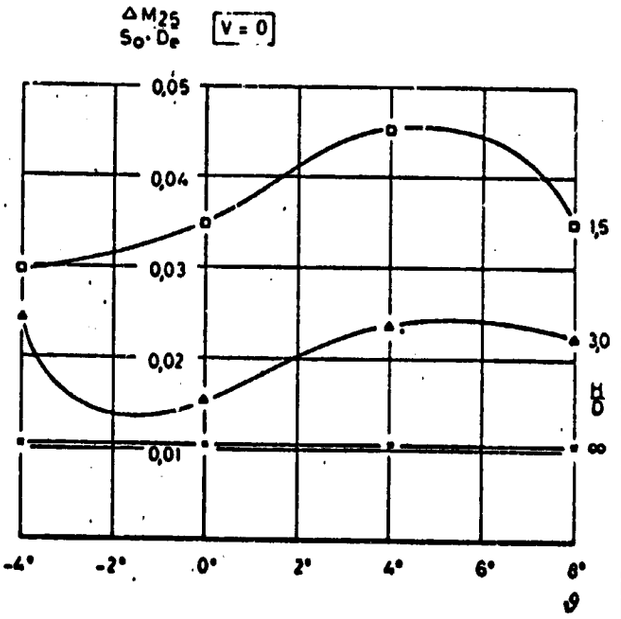

Config. B

[Commas represent decimal points]

52	Fig. 38	Comparison $\frac{\Delta M_{25}}{S_o \cdot D_e}$ Configs. A & B	HFB

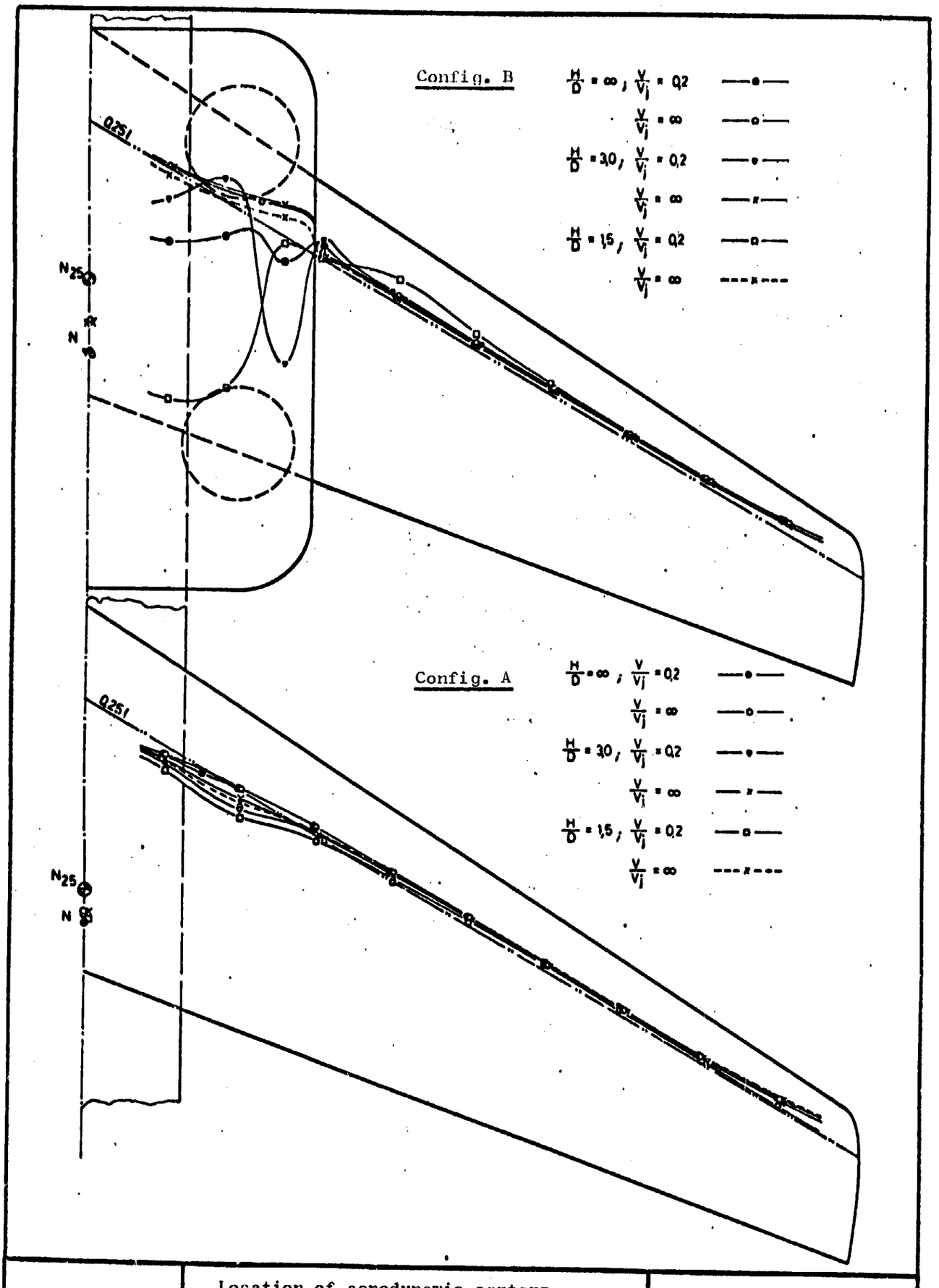

[Commas represent decimal points]

Fig.39 — Location of aerodynamic centers
Configs. A & B — HFB

Theory according to [6]
when $M_a = 0$ —o—o—
$M_a = 0{,}9$ —x—x—
measurement $Re \sim 7{,}6 \cdot 10^5$
when $M_a \sim 0$ ——
as per Figs. 10, 24

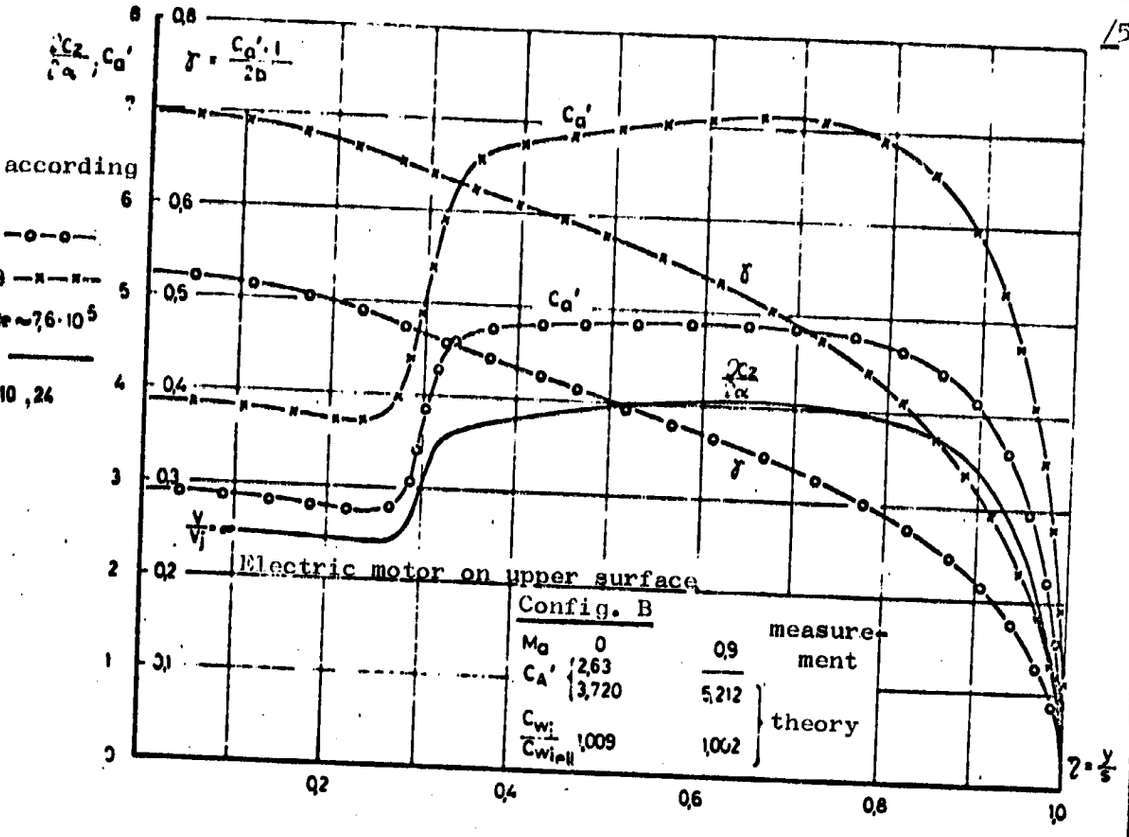

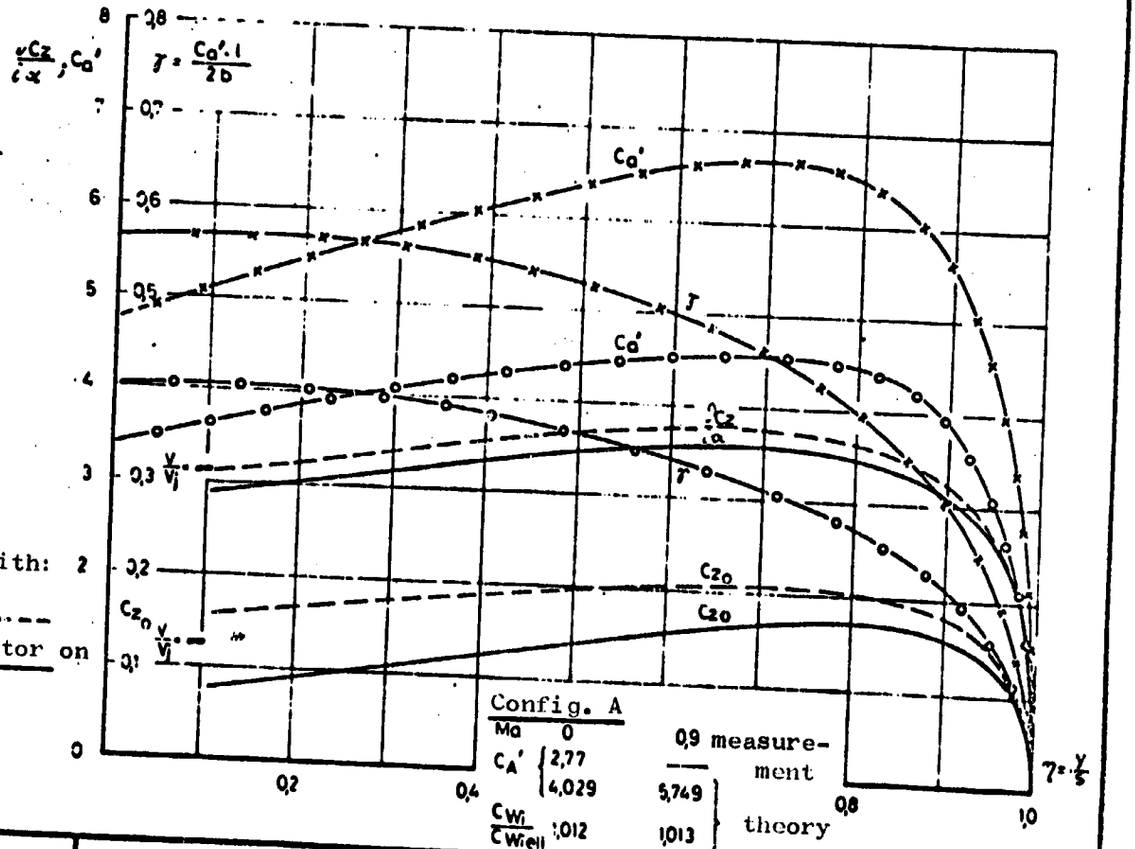

measured with:
no electric motor - - - - -
electric motor on upper surface ——

[Commas represent decimal points]

Fig. 40

Lift distributions Configs. A & B
Comparison with theory
Effect of electric motors

HFB